Influence of Land Surface Fluxes on Precipitation: Inferences from Simulations Forced with Four ARM–CART SCM Datasets

Y. C. SUD, D. M. MOCKO,* AND G. K. WALKER*

Climate and Radiation Branch, Laboratory for Atmospheres, NASA Goddard Space Flight Center, Greenbelt, Maryland

RANDAL D. KOSTER

Hydrological Sciences Branch, Laboratory for Hydrospheric Processes, NASA Goddard Space Flight Center, Greenbelt, Maryland

(Manuscript received 24 April 2000, in final form 23 February 2001)

ABSTRACT

Four different Atmospheric Radiation Measurement Program Cloud and Radiation Test Bed (ARM–CART) Single-Column Model (SCM) datasets were used to force an SCM in a number of simulations performed to study the influence of land surface fluxes on precipitation. The SCM employed Goddard Earth Observing System (GEOS-2) GCM physics, which includes a recent version of prognostic cloud scheme (Microphysics of Clouds with Relaxed Arakawa–Schubert), and a land model (Simplified Simple Biosphere Model) coupled to a highly resolved soil hydrological description in the vertical. The four ARM–CART datasets employed in these studies are referred as case 1, case 3, case 4, and case 8. The SCM simulation results broadly confirm the previous findings that an increase in the solar absorption and surface evaporation helps to increase the local rainfall, but they also reveal that the magnitude of the rainfall increase is strongly affected by the ability of the background circulation to promote moist convection. The simulated precipitation increase was as large as 50% of the evapotranspiration increase for case 1 that covered a relatively wet period. It was substantially reduced for cases 3 and 4 covering a normal rainfall period and became negligible for case 8, a dry case. A part of evaporation increase became horizontal divergence of water vapor; this would have the potential of increasing the precipitation downstream of the test region. For a particular background circulation, it was found that the evaporation–precipitation relationship, often defined as recycling ratio, is remarkably robust even for a large range of vegetation covers, soil types, and initial soil moistures. Notwithstanding the limitations of only one-way interaction (i.e., the large scale influencing the regional physics and not vice versa), the current SCM simulations show that recycling ratio is a function of the background circulation and not a regional and/or seasonal feature. Indeed, a vigorous biosphere can help to produce more rainfall under wet conditions but may do little to dislodge a large-scale drought. It is pointed out that even though these inferences are robust, they are prone to weaknesses of the SCM physics as well as the assumption of the large scale remaining unaffected by changes of moist processes.

1. Introduction

The earth's biosphere can influence surface moisture and energy fluxes through four primary controls, namely: (i) absorption of solar radiation within leaf organizations of vegetation canopies; (ii) evapotranspiration via access to root-zone soil moisture; (iii) stomatal control that naturally stifles evapotranspiration during warm and/or dry episodes; and (iv) altered surface roughness (on the scale of turbulent eddies), which acts to increase the boundary layer depth and cross-isobaric moisture convergence. In dry regions, scant vegetation leads to lesser transpiration and higher surface albedo, which in turn reduces solar absorption, land surface fluxes, and rainfall (e.g., Sud and Molod 1988; Dirmeyer and Shukla 1994). Likewise, removal of vegetation in any typical region can lead to reduction of evapotranspiration and/or land surface roughness and thereby to a decrease in rainfall (e.g., Sud and Smith 1985; Sud et al. 1988; Walker et al. 1995). A discernible dependence of rainfall on vegetation has been simulated and/or discussed in several papers (e.g., Dickinson 1980; Anthes 1984; Avissar 1992; Sud and Fennessy 1982, 1984).

The dependence of summer-season precipitation on biospheric processes can also be inferred from the first principles of moist convection as enunciated by Arakawa and Schubert (1974). The very same principles of moist convection have been used in the design of a

* Additional affiliation: General Sciences Corporation, Beltsville, Maryland.

Corresponding author address: Dr. Y. C. Sud, Climate and Radiation Branch, Laboratory for Atmospheres, Mail Code 913, NASA Goddard Space Flight Center, Greenbelt, MD 20771.
E-mail: sud@climate.gsfc.nasa.gov

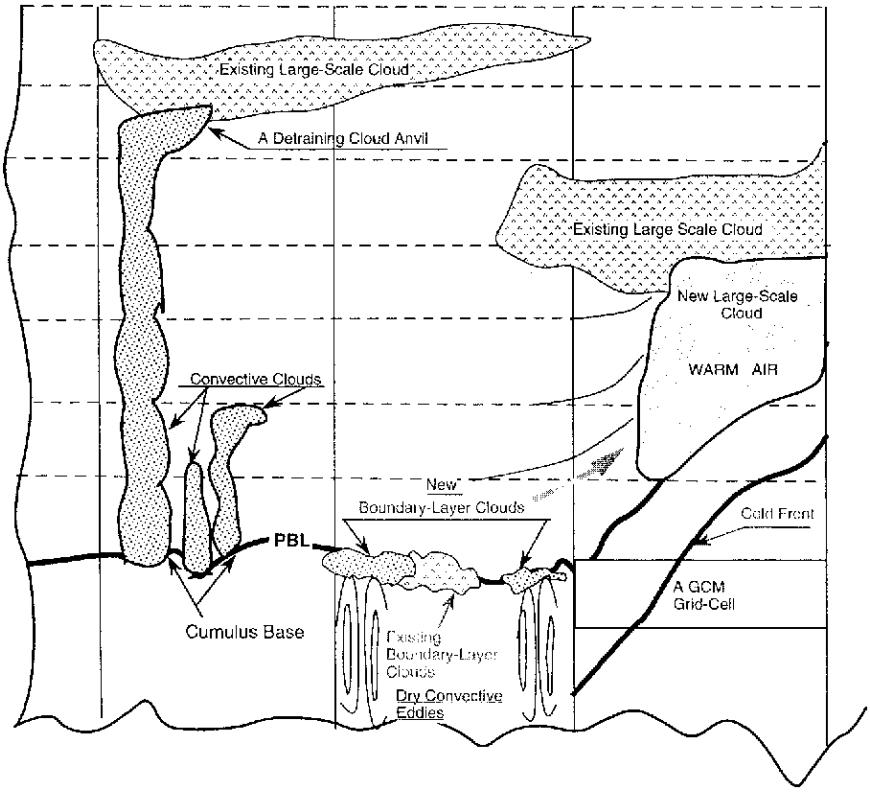

FIG. 1. Schematic representation of convective, stratiform, and boundary layer clouds in McRAS [adapted from Sud and Walker (1999)].

whole generation of physically based cumulus schemes, including relaxed Arakawa–Schubert (RAS; Moorthi and Suarez 1992) and Microphysics of Clouds with Relaxed Arakawa–Schubert (McRAS; Sud and Walker 1999). Sud et al. (1993, 1995) pedagogically argued and demonstrated that each vegetation process, when limited to affect the overlying column–atmospheric sounding, helps to promote moist convection. Specifically, a surface albedo increase leads to a near-surface energy deficit that reduces convective available potential energy (CAPE) and suppresses moist convection. Simulations in which the relative proportions of evapotranspiration and sensible fluxes [but not their sum (e.g., Sud et al. 1988)] are altered reveal that more evapotranspiration promotes more convective rainfall because it better enables CAPE accumulation before the moist convection gets ''turned on.'' Larger CAPE naturally enables moist convection to reach deeper into the atmosphere thereby producing more precipitation and associated atmospheric warming. Since convective (as opposed to stratiform) precipitation produces less fractional cloud cover, convective clouds allow more insolation to reach the surface of the earth, which naturally enhances the energy available for surface energy fluxes. Together with observational analyses (e.g., Otterman et al. 1990; Nicholson 1985; Skole and Tucker 1993) also suggesting precipitation enhancement by vegetation, such findings provide a rational physical basis for understanding the influence of vegetation on precipitation.

Pioneering GCM studies of Amazonian deforestation (e.g., Dickinson and Henderson-Sellers 1988; Henderson-Sellers et al. 1993) were performed to examine the impact of tropical rainforests on local precipitation. The outcome became rather ambiguous when results of sev-

TABLE 1. Soil types and parameters in the ISLSCP Initiative-I GEWEX GSWP dataset.

Soil type	Index	Porosity	ψ_s (m)	κ_s (m s^{-1})	B
Coarse—loamy sand	1	0.421	0.0363	1.41×10^{-5}	4.26
Medium coarse—sandy loam	2	0.434	0.1413	5.23×10^{-6}	4.74
Medium—loam	3	0.439	0.3548	3.38×10^{-6}	5.25
Fine medium—sandy clay loam	4	0.404	0.1349	4.45×10^{-6}	6.77
Fine—clay loam	5	0.465	0.2630	2.45×10^{-6}	8.17

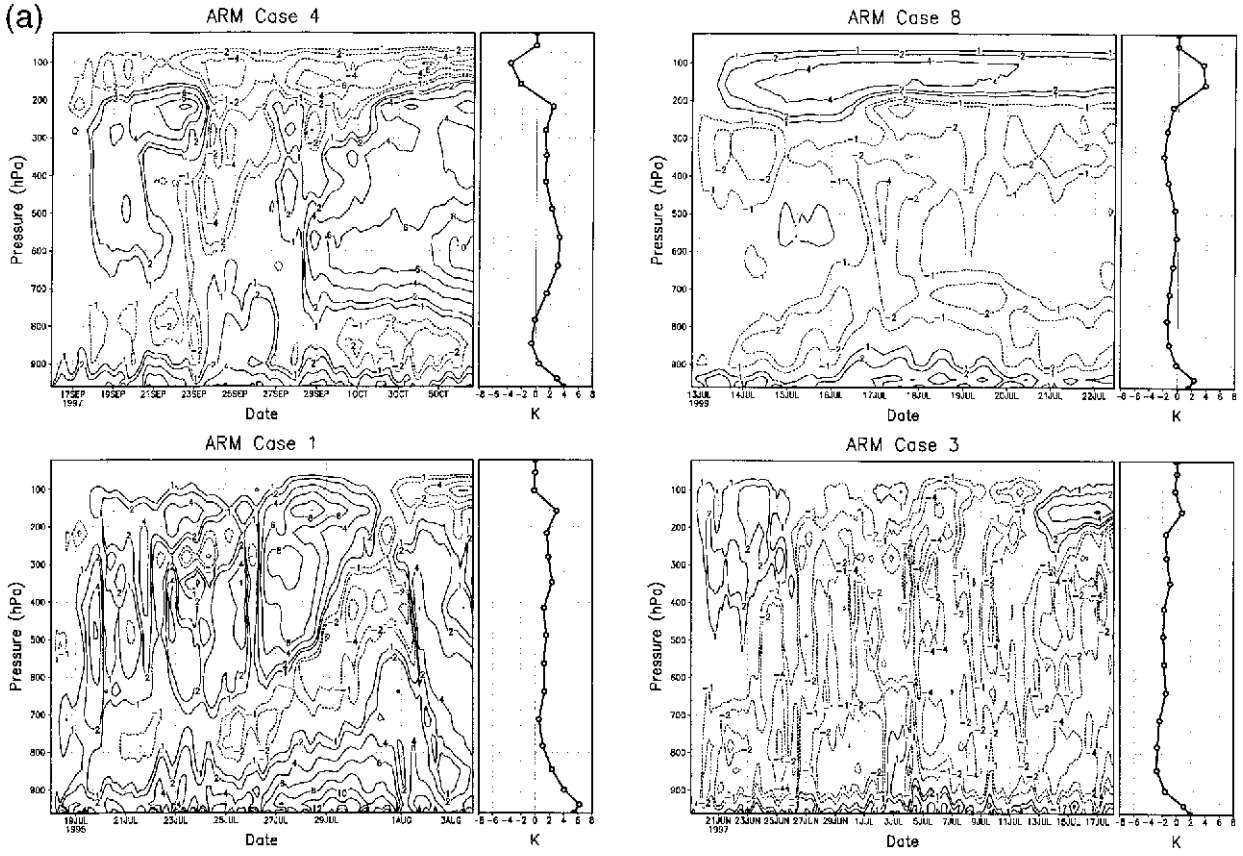

FIG. 2. SCM testing of McRAS with ARM–CART datasets for cases 1, 3, 4, and 8. (a)–(c) Simulation errors (simulation minus observed differences) for the temperature, specific humidity, and precipitation, respectively, for the SCM region using ARM–CART data forcings. Dashed contours are used for negative values. Observed precipitation is drawn dark solid in (c).

eral GCMs (each with its own interactive biosphere) were examined side by side. Table 1 of Hahmann and Dickinson (1997) shows a comparison of evapotranspiration, moisture convergence, and local rainfall simulated by 15 different GCMs that had been variously used to perform Amazon deforestation experiments. Although the majority of models simulated a substantial decrease in rainfall in response to deforestation, a few models simulated no change or even an increase in rainfall. Eltahir and Bras (1993) show that such differences are caused by the competing effects of (i) moisture convergence produced by the thermal heating of the lower troposphere and (ii) the moisture deficit caused by reduced evapotranspiration in deforestation. Clearly, some differences in the Hahmann and Dickinson (1997) comparison could be due to differences in the location and the extent of the imposed deforestation anomalies or in the simulated climatic index of dryness (Koster and Suarez 1999). Regardless of the reason for such large spreads among modeled inferences, the outcome tantamounts to poor overall understanding of vegetation–atmosphere interactions and cloud processes. Since models are expected to simulate the synthesized interactions among submodels, such model-to-model variations reveal lack of a satisfactory representation of modeled processes.

We submit that there is a fundamental need for (i) more extensive validation of modeled processes in GCMs and (ii) devising more ingenious ways of examining the land–atmosphere interaction problem to better isolate the fundamental processes and arrive at a better answer. One promising tool for analyzing land–atmosphere interactions is a Single-Column Model (SCM). An SCM uses best available estimate of observations [often generated from analysis of observations collected during an intensive observing period (IOP) or even a four-dimensional data assimilation analysis] to drive a particular column atmosphere. Therefore, an SCM has the ability to reveal the simulation accuracy as well as the importance of specific physical processes. We begin by examining the evidence of our SCM's performance in four Atmospheric Radiation Measurement Program Cloud and Radiation Test Bed (ARM–CART) data–forced simulations. Only after such evaluations are found to be satisfactory, will we attempt to use the SCM to analyze its response to biosphere–precipitation interactions.

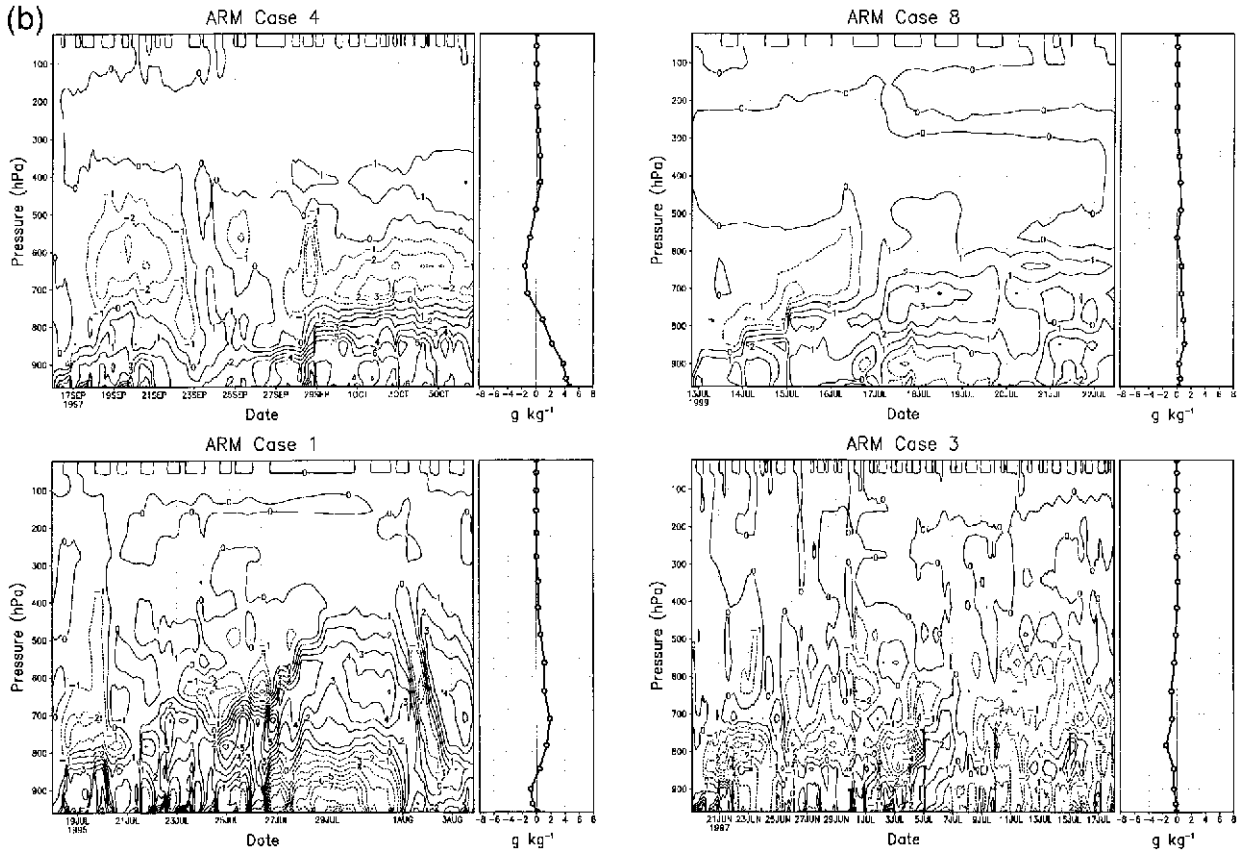

FIG. 2. (*Continued*)

We examine the influence of the biosphere on summer precipitation over the ARM–CART site of the midwestern Great Plains in the United States [for site details, see Randall and Cripe (1999, their Fig. 1, p. 24 531)]. This region is affected by strong moisture advection by the low-level jet, a manifestation of the large-scale forcing. Our SCM is coupled to Simplified Simple Biosphere Model (SSiB) for simulating biosphere–atmosphere interactions; SSiB in turn is coupled to a highly resolved 1D soil hydrological model that yields an accurate numerical solution of Richards's equation. The McRAS state-of-the-art cloud physics package is coupled to the Goddard Earth Observing System (GEOS-2) GCM physics and has been shown to produce realistic results (Sud and Walker 1999). Our goal is to simulate soil–vegetation–atmosphere interactions as realistically as possible. The lower hydrologic boundary condition is set 5 m below the surface of the land. Assuming that such a model is satisfactory for the Great Plains region, what could we learn about the response of the column atmosphere to changes in surface fluxes? The specific question we pose is if the large-scale atmosphere was essentially unaffected by much smaller scale changes in the land surface fluxes due to changes in vegetation cover or soil type or soil moisture, how would the vegetation–soil–rainfall interaction be affected locally? To answer this question, we force the SCM to interact with a suite of soil types, soil moistures, and/or vegetation cover fractions; we use four ARM–CART cases representing one wet rainfall, two near-normal, and one very dry period. For sensitivity evaluations, we perturb the boundary conditions. We will describe our SCM, the cloud scheme called McRAS, and the new 100-layer soil hydrological model in section 2. We will show some evidence of the intrinsic reliability of the SCM's physics in section 3. We will then show key results of SCM studies with four ARM–CART datasets using five soil types and a full range of soil moisture and vegetation covers in section 4. The broader implications of our findings are discussed in section 5.

2. Single-column model

SCMs have a long history of use for evaluating physical submodels representing boundary layer processes (e.g., Hoffert and Sud 1976), land surface hydrology (Koster and Eagleson 1990), and moist processes including convection and downdrafts (e.g., Cheng 1989). Randall et al. (1996) discussed a variety of innovative uses of SCMs and illustrated how an SCM could be a useful device for model parameterization evaluation and/or scientific hypothesis validation. We will use our

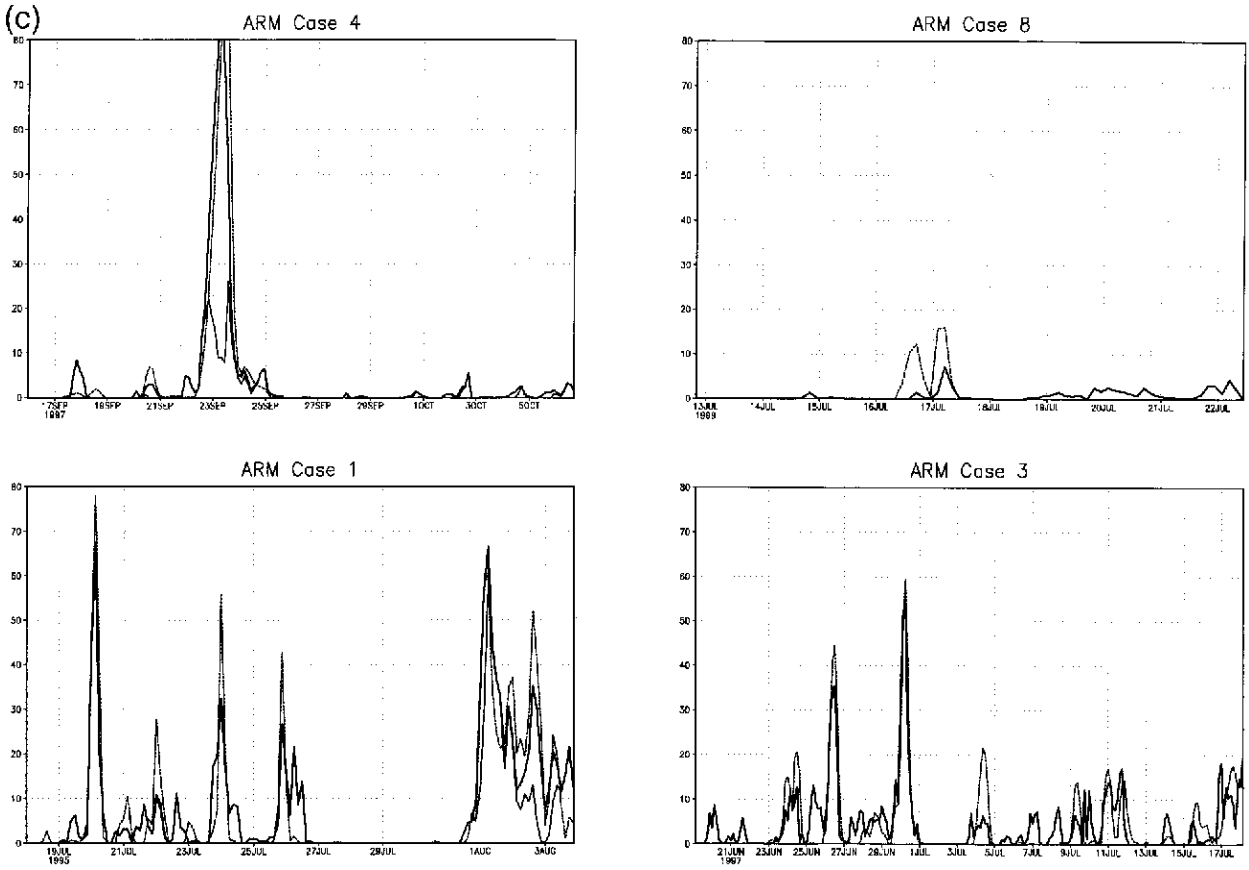

FIG. 2. (*Continued*)

SCM to validate the hypothesis that land surface biospheric processes, particularly evapotranspiration, have a positive feedback effect on convective precipitation. Our earlier findings (Sud et al. 1993, 1995) were that all biospheric processes help to promote local rainfall, particularly the convective type. Since the inferences were based on global soundings, they are expected to hold for the midwestern United States typified by the ARM–CART site. However, the magnitude of this feedback was not discerned in those findings. To estimate the magnitude of these feedbacks as well as to reevaluate the earlier findings, we propose to force our SCM with the ARM–CART SCM data. Comparison of simulations with observations will help us to better differentiate between the mathematical and/or numerical characteristics of our parameterization vis-à-vis the reality of the atmosphere.

Our SCM has been extensively described in Sud and Walker (1993), who used it for evaluating the design of a convective downdraft scheme using Global Atmospheric Research Program Atlantic Tropical Experiment (GATE) Phase-III data. More recently, Sud and Walker (1999) used the same SCM to evaluate the performance of a new McRAS. In these evaluations, there were virtually no time-mean biases. The ARM–CART SCM datasets are more recent and comprehensive. Several modeling groups are using these datasets internationally. Recently, ARM–CART case-1 data were used for model intercomparison (Ghan et al. 2000). Our SCM did a fairly reasonable job of simulating time histories of temperature, humidity, and precipitation. The simulated atmospheric lapse rates were also reasonable except for some discernible errors in the boundary layer. These errors have been of some concern, but given that the SCM's lapse rates are bracketed between the dry and moist adiabatic, whereas the observations are not, the boundary layer lapse rate differences remain a puzzle to date.

Randall and Cripe (1999) discussed three different ways in which an SCM can be used for testing physical parameterizations. In the very basic form, that is, without flux adjustments or artificial relaxation, which the authors call ''Revealed Forcing'' [also baseline case of Ghan et al. (2000)], the specific humidity q tendency of the atmosphere is expressed by

$$\frac{\partial q}{\partial t} = -\left(\nabla \cdot Vq + \frac{\partial \omega q}{\partial p}\right) + P. \qquad (1)$$

Here $\nabla \cdot Vq$ is the domain-averaged horizontal, and $\partial \omega q/$

∂p is the domain-averaged vertical, flux divergence tendency of q. All modeled physical processes are folded into the P tendency, the last term of (1). Clearly, the flux forms of moisture transports contain the sum of advective plus divergent tendencies. Equation (1) can now be recast with q split three ways: (i) as observed, q_{obs}; (ii) as affected by the time-integrated influence of land surface fluxes (lsf), q'_{lsf}; and (iii) as affected by the time-integrated influence of SCM errors, q'_{me}, yielding

$$q = q_{\text{obs}} + q'_{\text{lsf}} + q'_{\text{me}}. \tag{2}$$

On substitution and dropping primes for clarity, (1) becomes

$$\frac{\partial q}{\partial t} = -\left(\boldsymbol{\nabla} \cdot Vq_{\text{obs}} + \frac{\partial \omega q_{\text{obs}}}{\partial p}\right) - \left(\boldsymbol{\nabla} \cdot Vq_{\text{lsf}} \frac{\partial \omega q_{\text{lsf}}}{\partial p}\right) - \left(\boldsymbol{\nabla} \cdot Vq_{\text{me}} + \frac{\partial \omega q_{\text{me}}}{\partial p}\right) + P. \tag{3}$$

The observed tendency can also be written in the advective form, which merely alters the first term on the rhs to give

$$\frac{\partial q}{\partial t} = -\left(V \cdot \boldsymbol{\nabla} q_{\text{obs}} + \omega \frac{\partial q_{\text{obs}}}{\partial p}\right) - \left(\boldsymbol{\nabla} \cdot Vq_{\text{lsf}} + \frac{\partial \omega q_{\text{lsf}}}{\partial p}\right) - \left(\boldsymbol{\nabla} \cdot Vq_{\text{me}} + \frac{\partial \omega q_{\text{me}}}{\partial p}\right) + P. \tag{4}$$

A simulation without vegetation or soil-type anomalies will have only the first and third terms contained in square brackets on the rhs, plus its tendency due to physical adjustment, P_{cont}. The anomalous land surface fluxes of our study will have all the three terms affecting the tendency, plus its influence on the physical adjustment term, P_{lsf}. By appropriately accounting for these contributions, we can delineate the land surface (vegetation and/or soil) fluxes anomaly influence on precipitation changes represented in P_{lsf}.

First let us recast (4) in the following forms:

$$\frac{\partial q}{\partial t} = -(\text{OAT}) - \left(\boldsymbol{\nabla} \cdot Vq_{\text{me}} + \frac{\partial \omega q_{\text{me}}}{\partial p}\right) + P_{\text{cont}}, \tag{5}$$

$$\frac{\partial q}{\partial t} = -(\text{OAT}) - \left[\boldsymbol{\nabla} \cdot V(q_{\text{me}} + q_{\text{lsf}}) + \frac{\partial \omega (q_{\text{me}} + q_{\text{lsf}})}{\partial p}\right] + P_{\text{lsf}} + P_{\text{cont}}, \tag{6}$$

where (OAT) is the observed advective tendency. The implied constancy of V and ω must be remembered. The control simulations can be performed with the SCM using observed advective tendencies from the ARM–CART observations [so-called (OAT) term] plus model errors. In the anomalous surface-flux simulations, they get modulated by the q_{lsf} and P_{lsf} terms on the rhs of (6), which represents the sum of model errors and anomalous vegetation and/or soil-type modification influences. If the simulation can be assumed to be realistic (i.e., not far removed from plausible observations), then anomaly-minus-control differences will counter the model errors. This is particularly true for errors that produce a linear response in the simulation. By subtracting simulation (5) from (6), we can hope to isolate lsf-forced tendencies. This is a modification of the artificial relaxation methodology of Randall and Cripe (1999) in which the advective equations have been recast to delineate the influence of surface fluxes on the ensuing changes in the SCM simulations.

The second term in (5) and (6) represents the horizontal and vertical advective tendencies that are specific to the control and vegetation and/or soil anomaly simulations. To estimate them, we use the grid-cell domain-averaged horizontal wind V and vertical pressure velocity ω from observations. Both of them are explicitly provided in the ARM–CART SCM data. The second term can further be expressed as

$$\frac{\partial q_{\text{hor}}}{\partial t} = -\frac{V_{\text{obs}} \cdot \boldsymbol{\nabla}(q_{\text{mod}} - q_{\text{obs}})}{\Delta x} - (q_{\text{mod}} - q_{\text{obs}})\boldsymbol{\nabla} \cdot V_{\text{obs}}, \tag{7}$$

where ΔX is the horizontal length scale of the domain, while the observed wind V_{obs} is taken to be constant. Here q_{mod} generically refers to the model-generated q, which is different from q_{obs} due to model errors and/or vegetation anomaly influences, as stated before.

The second part for the vertical flux divergence of q is of the form

$$\frac{\partial q_{\text{vert}}}{\partial t} = -\frac{\Delta \omega_{\text{obs}}(q_{\text{mod}} - q_{\text{obs}})}{\Delta p}. \tag{8}$$

Here ω_{obs} is a function of p and must be multiplied with q anomaly to conserve the anomalous moisture flux in the entire column in the course of ensuing vertical advection. If we run all the cases involving different vegetation covers and soil types by invoking (7) and (8) with or without including vegetation/soil modification effects, the influence of vegetation and/or soil type on the parameterized physical interactions and observed advective tendency of q will be revealed. Whenever q of the SCM is different from the observed, the q advected (in the horizontal and vertical directions) will get modified. The formulas are conceptually similar to that of Randall and Cripe (1999), except that our time constant τ_{hor} is simply

$$\tau_{\text{hor}} = \frac{\text{horizontal grid length scale}}{\text{horizontal wind velocity}}. \tag{9}$$

A parallel equation can be written for tendencies of other conserved quantities being advected of which potential temperature Θ is most relevant. In the GEOS GCM, we advect cloud fraction and cloud water too;

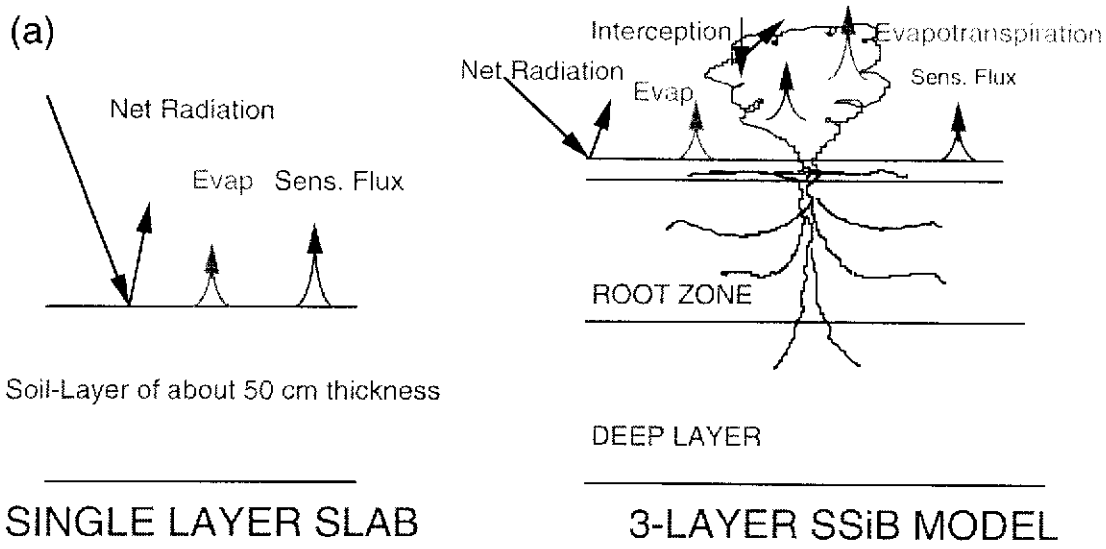

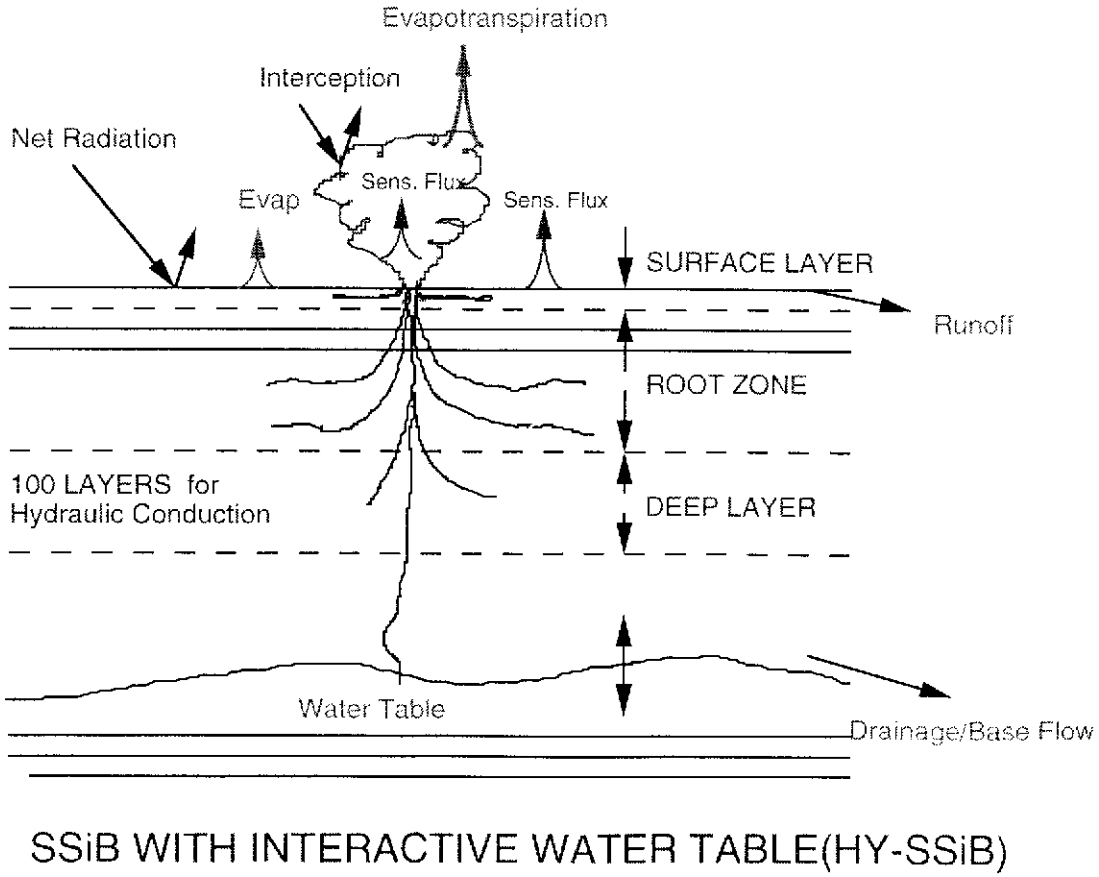

FIG. 3. (a) Schematic coupling of a 100-layer soil hydrological description and SSiB with fluxes. (b) Soil types in ISLSCP Initiative-I data depicted in the three-component mixture viewed as soil triangle. Typical mixing ratios of the soils for different soil types are located in the triangle.

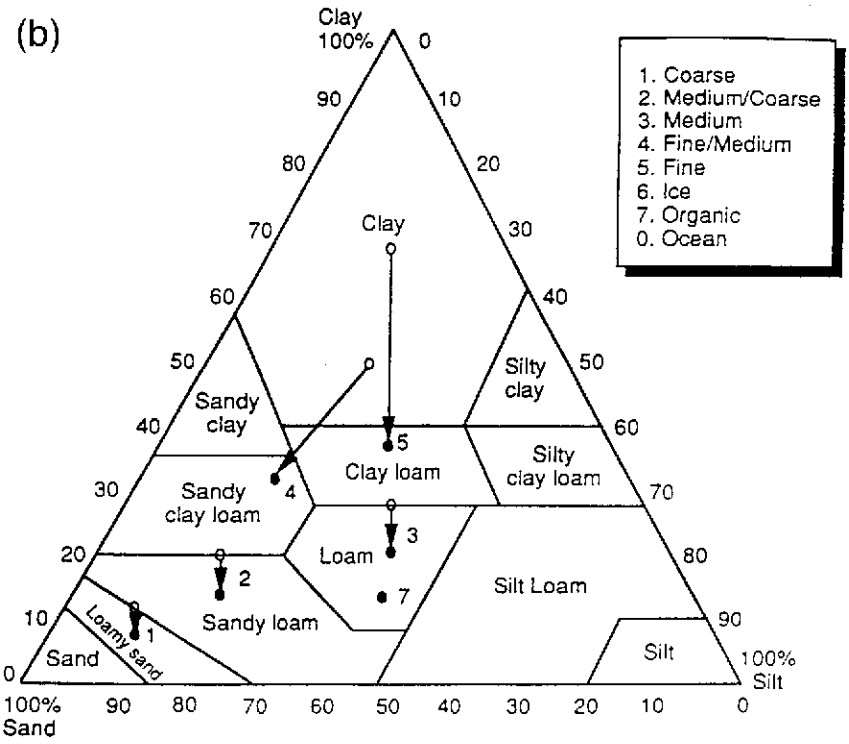

FIG. 3. (*Continued*)

nevertheless, without the lateral cloud forcing, it is not possible to conduct them in an SCM environment. Since both q and Θ are influenced by surface processes, we must perform an appropriate adjustment for both variables.

a. Cloud model (McRAS)

The cloud model of our SCM is called McRAS. It was designed with the aim of simulating prognostic moist processes, clouds, and cloud–radiation interactions in GCMs. McRAS distinguishes and parameterizes three types of clouds: convective, stratiform, and boundary layer, as shown schematically in Fig. 1. The RAS scheme of Moorthi and Suarez (1992) generates convective clouds; however, the cloud microphysics and stratiform and boundary layer cloud schemes follow Sud and Walker (1999). The simulated convective clouds transform and merge into stratiform clouds on a 1-h timescale, while the boundary layer clouds merge into the stratiform clouds in the same time step. The cloud condensate converts into precipitation following the autoconversion equations of Sundqvist (1988, 1993) and Sundqvist et al. (1989), which contain a parametric adaptation for the Bergeron–Findeisen process of ice crystal growth and collection of cloud condensate by precipitation. All SCM clouds convect, advect, and diffuse vertically (but not horizontally) with a fully interactive cloud microphysics. In this way, the life cycle of a cloud is inferred from cloud dynamics and microphysics, whereas the optical properties are derived from the statistical distribution of hydrometeors in idealized cloud geometry. Using the SCM (described above) with the GATE Phase-III data, Sud and Walker (1999) showed that, together with the rest of the model physics, McRAS reproduces the observed temperatures, humidities, and precipitation rates without discernible systematic errors. The time histories and time means of in-cloud water and ice distribution, fractional cloudiness, cloud optical thickness, origin of precipitation in the convective anvils and towers, and the convective updraft and downdraft velocities and mass fluxes were all simulated reasonably well, even though they could not be verified with the available data. For such evaluations, observational data on horizontal advection of clouds and incloud water is needed and so far it is not available.

To determine the suitability of McRAS–SCM in the ARM–CART environment, McRAS–SCM was integrated for each of four ARM–CART SCM datasets: cases 1, 3, 4, and 8, which span 2–4 weeks of IOP in June, July, and September months. These test integrations were performed in a prognostic mode without any adjustment for the model biases; that is, the horizontal advective tendency and the rates of surface fluxes were prescribed from observations. The results are shown in Figs. 2a–c. Two cases are warmer and two are colder than observed in the time mean (Fig. 2a). The specific humidity biases also are dissimilar among the cases (Fig.

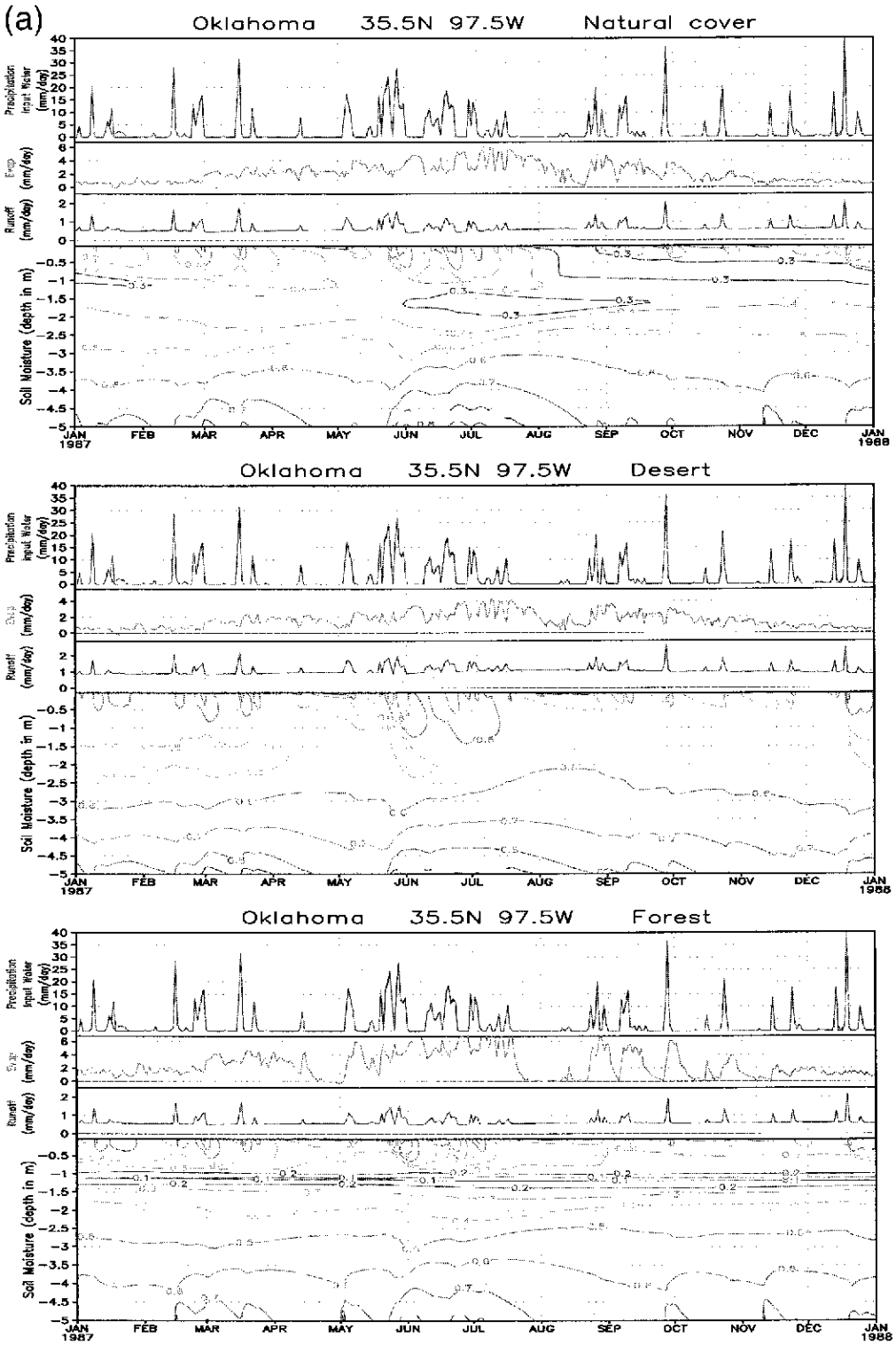

FIG. 4. Influence of vegetation cover on the hydrological and surface fluxes simulated with 1987 ISLSCP Initiative-I data of the Oklahoma region (a surrogate for the ARM–CART site). (a) Actual fields, and (b) vegetation anomaly minus control differences. The grid cell is 1° lat × 1° long with location of its center given at the top of each map.

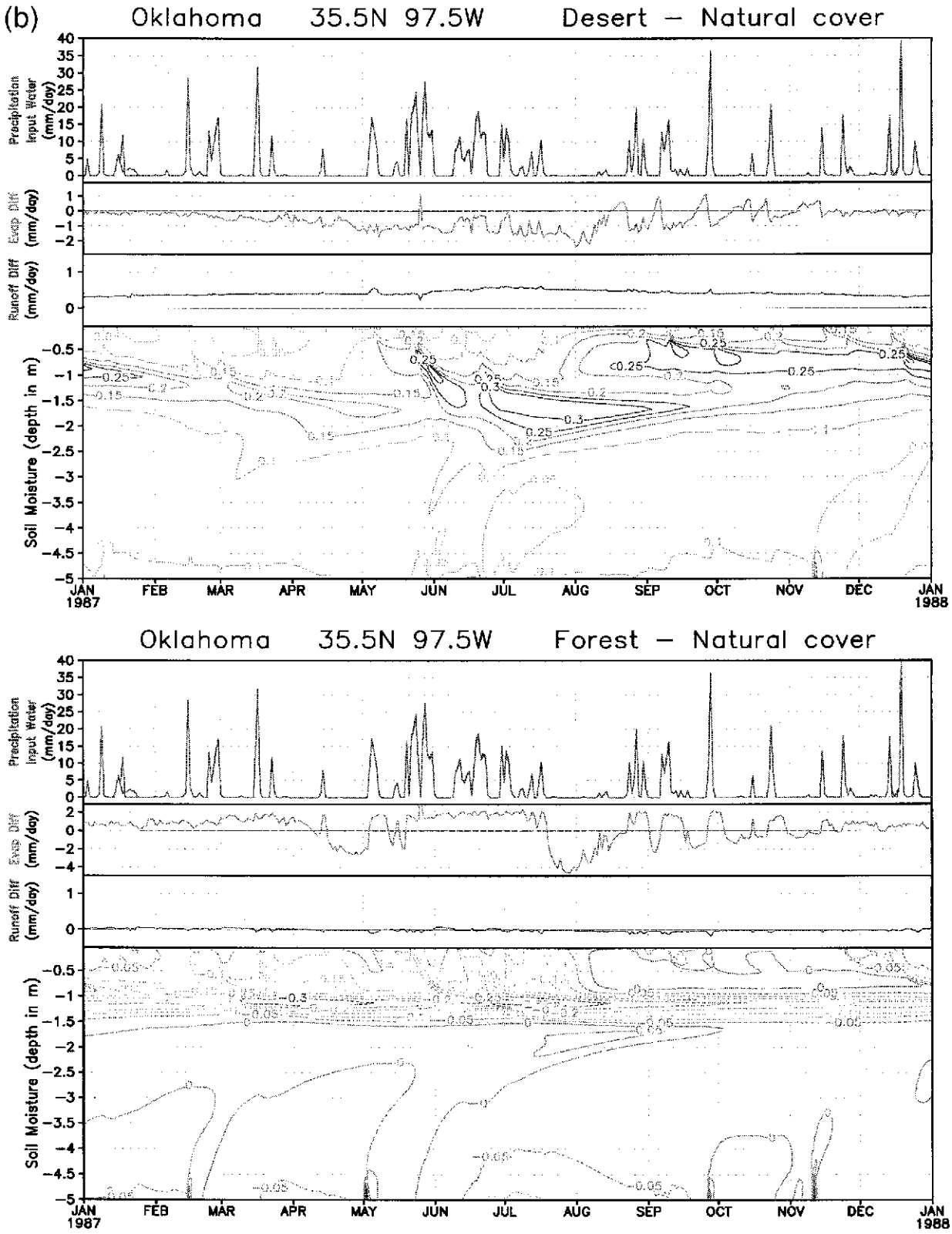

FIG. 4. (*Continued*)

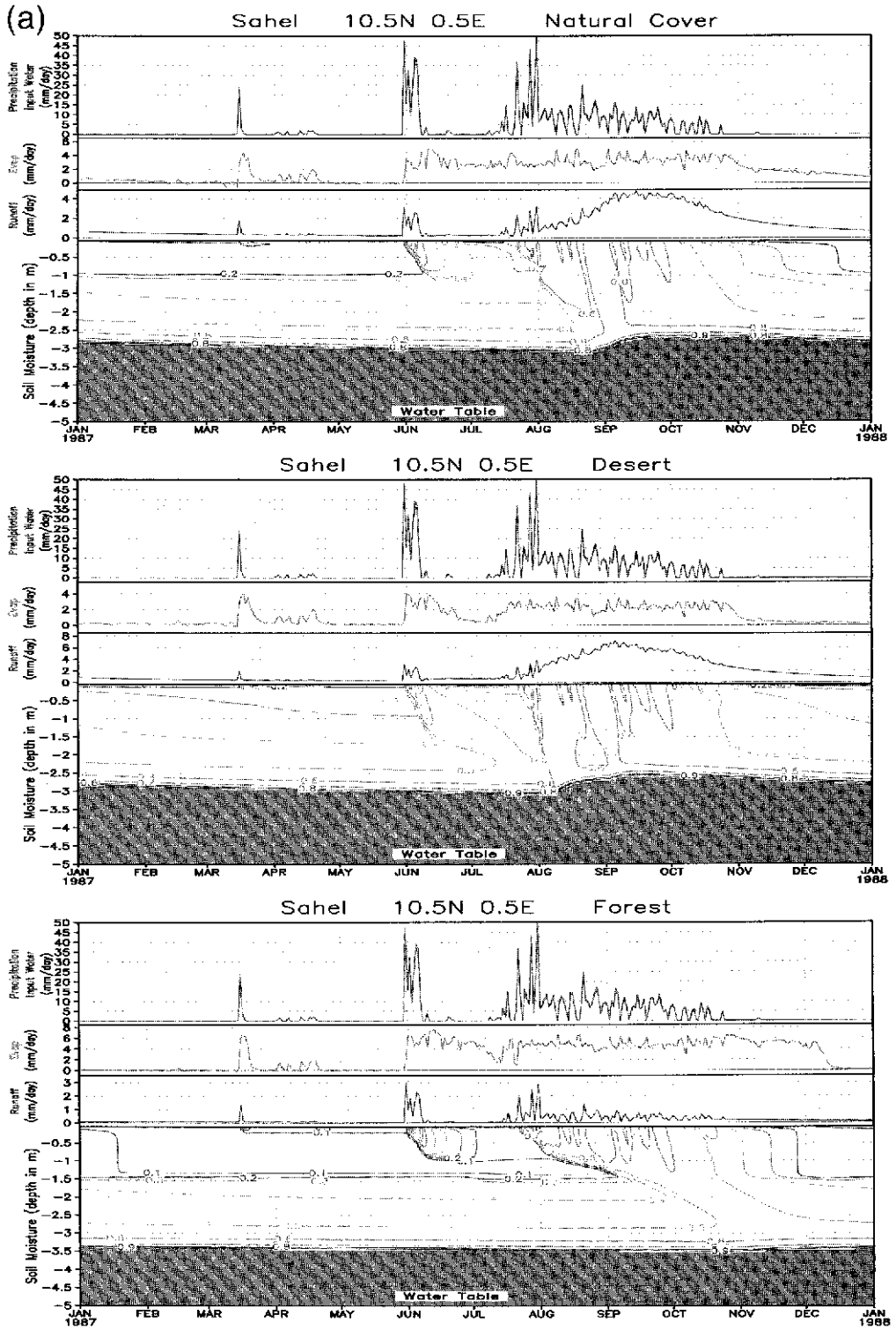

FIG. 5. Same as Fig. 4 but for the Sahel location.

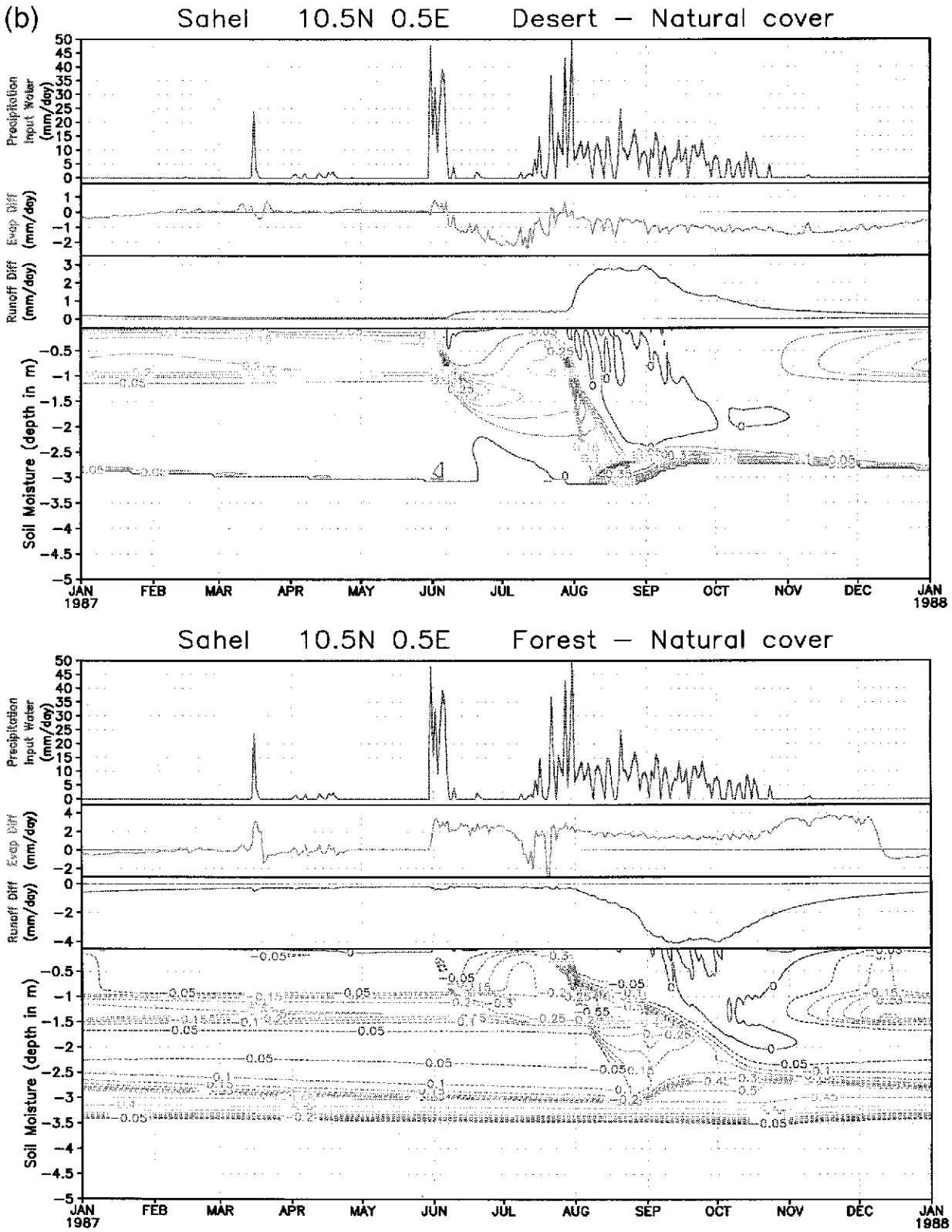

FIG. 5. (*Continued*)

2b). Case 1 is wetter than normal and its simulated precipitation tracks the observed quite well (Fig. 2c). Case 8 is extremely dry, and the simulated precipitation is distributed in time as compared with two small episodes in the observations. A few notable systematic errors of this evaluation are as follows. All the simulated near-surface temperatures were a few degrees warmer than observed and produce a lapse rate much stronger than that observed between the surface and 800 hPa. However, there is no similarity in the temperature biases in the rest of the atmospheric column. Although essentially similar to the observed, the SCM simulations also produced somewhat lesser rainfall than observed. We shall show later that the SCM produces realistic time-mean evapotranspiration; therefore any biases (observed minus SCM-simulated) in the time-averaged rainfall must result from a lack of moisture conservation in the ARM–CART SCM data or the humidity biases of the simulated SCM sounding at the end of the integration. Nevertheless, we must contend with these errors for now.

b. Land model

Our land model is the SSiB. It is described in Xue et al (1991). A brief discussion of several upgrades to SSiB of our SCM can be found in Mocko and Sud (2001). An additional modification to land hydrology is worthy of discussion. The original SSiB had three soil layers and parameterized interlayer hydraulic conduction with several arbitrary limits on Richards's equation, which, in a crude way, produced reasonable vertical fluxes. For the current exercise, we needed a more accurate solution of the Richards equation. Consequently, we solved the soil hydraulic conduction equation with much higher vertical resolution using a numerical methodology developed by Koster et al. (2000). After experimenting with 1-cm vertical resolution and 500 layers in the vertical, we eventually settled on a 100-layer model with 5-cm vertical resolution (Fig. 3a) without any loss of accuracy. In this design, plant roots are equally distributed among the layers that contain them. This resolution is not suitable for GCM work, but it is vital for accurate hydraulic conduction in the vertical for land assuming no subgrid-scale variability. Clearly, lack of adequate representation of subgrid-scale variability in the horizontal is a limitation, but that is a separate issue, and we postpone its treatment for a later time. Nevertheless, the 100-layer soil model has the bottom boundary at 5-m depth, whereas the vegetation (root zone) layers of SSiB can vary regionally as a function of soil type and vegetation covers. The original SSiB was evaluated with the International Satellite Land Surface Climatology Project (ISLSCP) Initiative-I data under the Global Soil Wetness Project (GSWP; Dirmeyer et al. 1999) as well as against other simple land schemes (Mocko and Sud 1998). The GSWP surface forcing dataset covers a period of 24 months: 1 January 1987–31 December 1988. In these data, the world was characterized by only five soil types (Table 1, Fig. 3b) and 10 different biomes; nevertheless, in the SSiB design a grid cell can be assigned only one soil type and one biome. In other words, tiling is not feasible. However, some horizontally homogeneous grid-scale variability can be invoked through the choice of fractional vegetation cover and leaf area index. The new 100-layer model was extensively tested with ISLSCP Initiative-I data without use of any tuning factors for a range of conditions varying from extremely dry to highly moist. The model generates reasonable soil water transport timescales for all soil types and parameterized vegetation processes.

As an example, we show in Fig. 4a how altering the vegetation in the GSWP evaluation (near the ARM–CART site) from a fully vegetated ground cover to a desert would affect the simulated soil moisture and land hydrology. Desert conditions lead to less evaporation and higher soil moisture and soil water drainage or runoff, whereas full vegetation cover produces more evaporation and less soil moisture and runoff. Such differences are also evident in the difference maps (Fig. 4b). Without vegetation removing soil water by transpiration, the soil moisture fraction in the month of June, for example, at 1–1.5-m depth (top panel, Fig. 4a) becomes as high as 0.6 versus only about 0.3 for the simulation with natural vegetation cover. With 99% vegetation cover (or ''forest''), there is a systematic reduction of soil moisture, particularly in the spring season in which there is considerable soil water uptake by transpiration. However, in late summer, the soil moisture does not drop much below 0.3 for the natural ground cover, because once vegetation starts to wilt, it does not produce very much transpiration. Similar results can be noted for Sahel, which has an extended dry period before the onset of the summer monsoon (Figs. 5a,b). At the beginning of the rainy season, the soil wetting time for the deep soil is on the order of 10–20 days as can be seen from the slope of the soil moisture isohalines going into the deeper regions of the soil. Once wetted, the adjustment timescale is much smaller. Regardless, wetter (drier) soil up to 3-m depth is simulated for minimal (maximal) vegetation cover simulations. In these assessments, the forcing of the land surface by rainfall and near-surface atmospheric conditions is maintained invariant. Similar assessments were produced for monsoonal India, Mississippi basin, and over a dozen other regions of the world (not shown). In all of these regions, the land hydrology and land surface fluxes simulated a very reasonable behavior (which is an evidence of an accurate numerical calculation of Richards's equation), although observational verification could not be performed because of lack of in situ data. Having satisfied ourselves of a reasonable performance of the soil hydrological model, we linked this 100-layer soil SSiB model to the atmospheric SCM to conduct the vegetation–soil–atmospheric interaction studies.

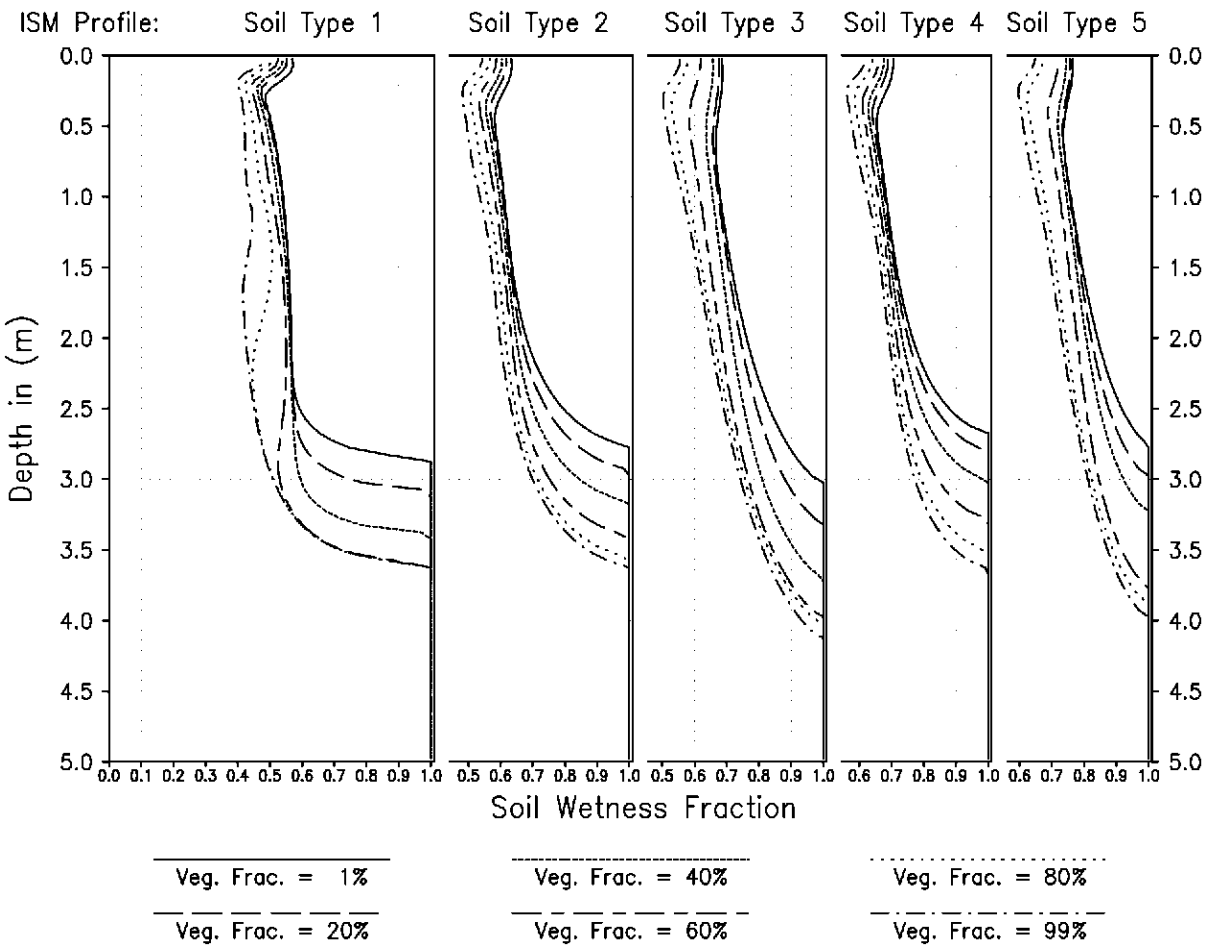

FIG. 6. Thirty initial soil moisture profiles used for case 1. Soil moistures were produced by running each of the five soil types with each of the six vegetation covers of the ARM–CART simulation using ISLSCP Initiative-I forcing data from 1 Jan up to the starting date for the GSWP data for 1987.

3. Design of the experiment

To evaluate the influence of vegetation on rainfall in the midwestern United States, we employ ARM–CART–SCM data over the ARM–CART site (a 300 km $\times$ 300 km region in Kansas and Oklahoma). The ARM–CART data used in this investigation were collected in four IOPs referred to as case 1 (18 July–4 August 1995), case 3 (19 June 1997–18 July 1997), case 4 (15 September 1997–6 October 1997), and case 8 (12 July 1999–22 July 1999). At the time of writing this paper, case 8 was not assigned an official number. The ARM–CART measurements also provide surface fluxes, top-of-the-atmosphere radiative inputs, and advective and divergent heat, moisture, and momentum tendencies for the SCM atmosphere at 16 levels. The observations were analyzed in 4D variational assimilation (Zhang and Lin 1997) and made available at 3-h intervals. The ISLSCP Initiative-I data in the ARM–CART region indicate roughly 60% vegetation cover for July; however, we allowed the vegetation cover to vary from 1% to 99% in order to delineate the influence of vegetation on simulated rainfall. Our experiment is the SCM equivalent of a regional modeling experiment in which the large-scale forcing is prescribed at the lateral boundaries from analysis of observations while the chosen region is free to respond with changes in its surface fluxes and atmospheric adjustments. The main difference is that here the SCM employs GCM grid-scale parameterizations to represent changes in mesoscale circulation. The influence of vegetation on surface fluxes as well as temperature and humidity soundings gets communicated in the vertical through physical processes, namely, turbulence, dry convection, and moisture–cloud-radiative forcing of the column atmosphere. Clearly, we also have the freedom to alter the soil type and soil moisture dependent hydraulic properties. Since ISLSCP Initiative I endorsed five possible soil types for all land throughout the world, and recognizing the possibility of large variations in soil types in a typical 300 km $\times$ 300 km size of land, we evaluated the performance of the SCM with each soil

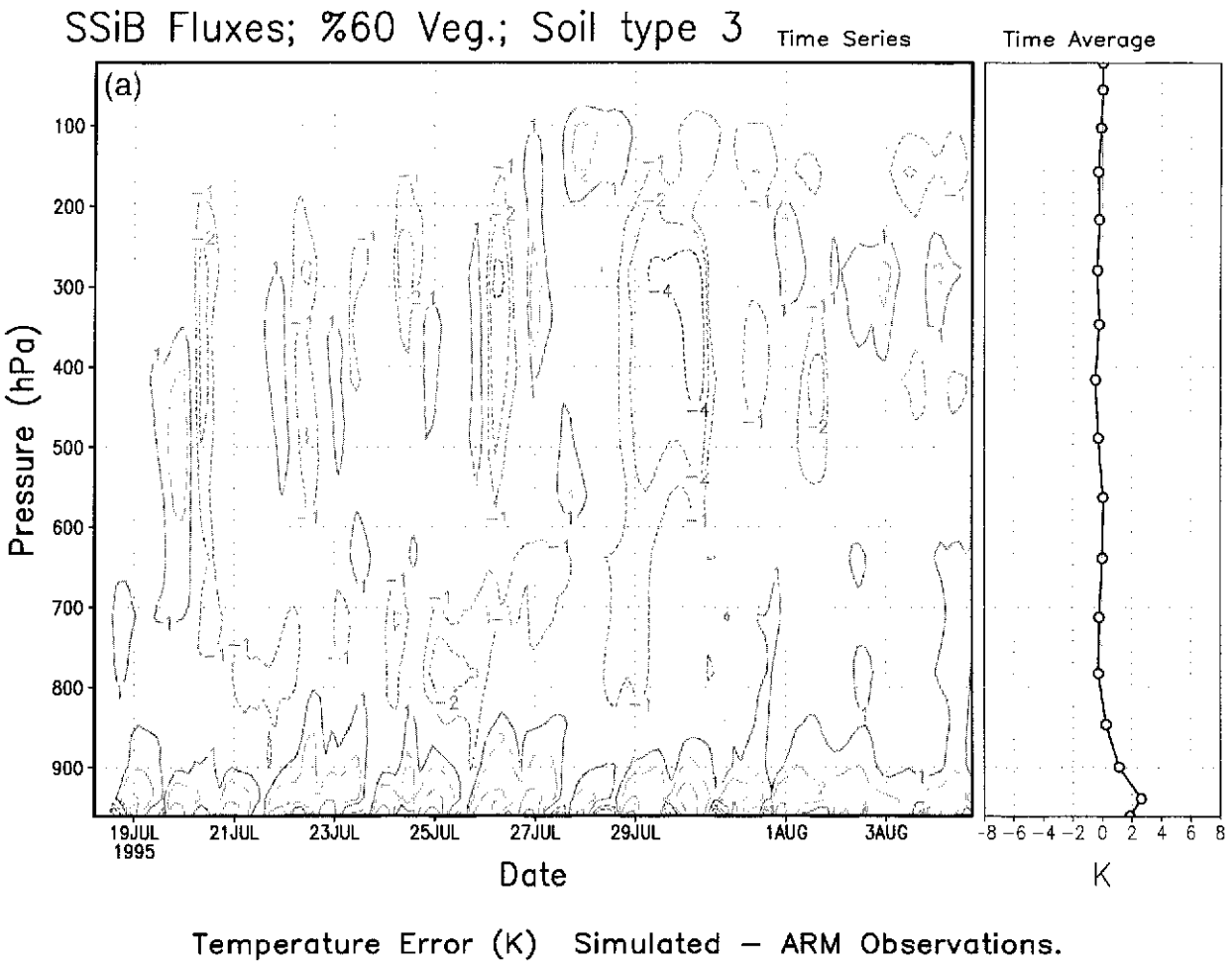

FIG. 7. Case-1 simulated errors (simulated minus observed) for the control with soil type 3 and vegetation cover of 60% with corrections for the model errors: (a) temperature fields, (b) humidity fields, and (c) simulated (dashed) vis-à-vis observed (dark solid) precipitation.

type using the same observed forcings. Six-months-or-longer spinup integrations performed with ISLSCP Initiative-I data for 1987, which provide the initial soil moisture profiles for the SCM evaluation period, were needed for a reasonable equilibration between soil water and precipitation. The method produced reasonable soil moisture profiles. This is a compromise because the forcing data for the antecedent periods of 1995 and other years were unavailable. In fact, keeping the same forcing leads to more soil moisture for less vegetation cover because with less vegetation there is less transpiration. We performed the same set of simulations for each of the four ARM–CART datasets. For each ARM–CART dataset, we ran a suite of 30 ($= 6 \times 5$) simulations, representing all combinations of six vegetation covers (namely, 1%, 20%, 40%, 60%, 80%, and 99%) and five soil types. The SCM-derived initial soil moisture profiles for the control cases for case 1 are given in Fig. 6. We then produced four additional ensemble of thirty simulations each, in which the initial soil moisture profile of the 60% vegetation cover for each soil type was varied to introduce additional soil dryness of 25%, 50%, 75%, and 100% of the soil moisture deficit ($= 1 - f_s$), where f_s is the soil moisture. Thus 150 simulations for each ARM–CART case were performed, which becomes $150 \times 4 = 600$ simulations altogether for four ARM–CART cases. These simulations were used to analyze the relationships among soil moisture, soil type, vegetation cover, and rainfall.

4. Results

The objective of the current study is to determine the influence of vegetation on the rainfall. These simulations are directly relevant to the hydrometeorological conditions in the midwestern United States. We used the ARM–CART data to perform SCM simulations in which the initial soil moisture profile was varied by soil type as described in section 3. All these cases were used to address the influence of initial soil moisture profile

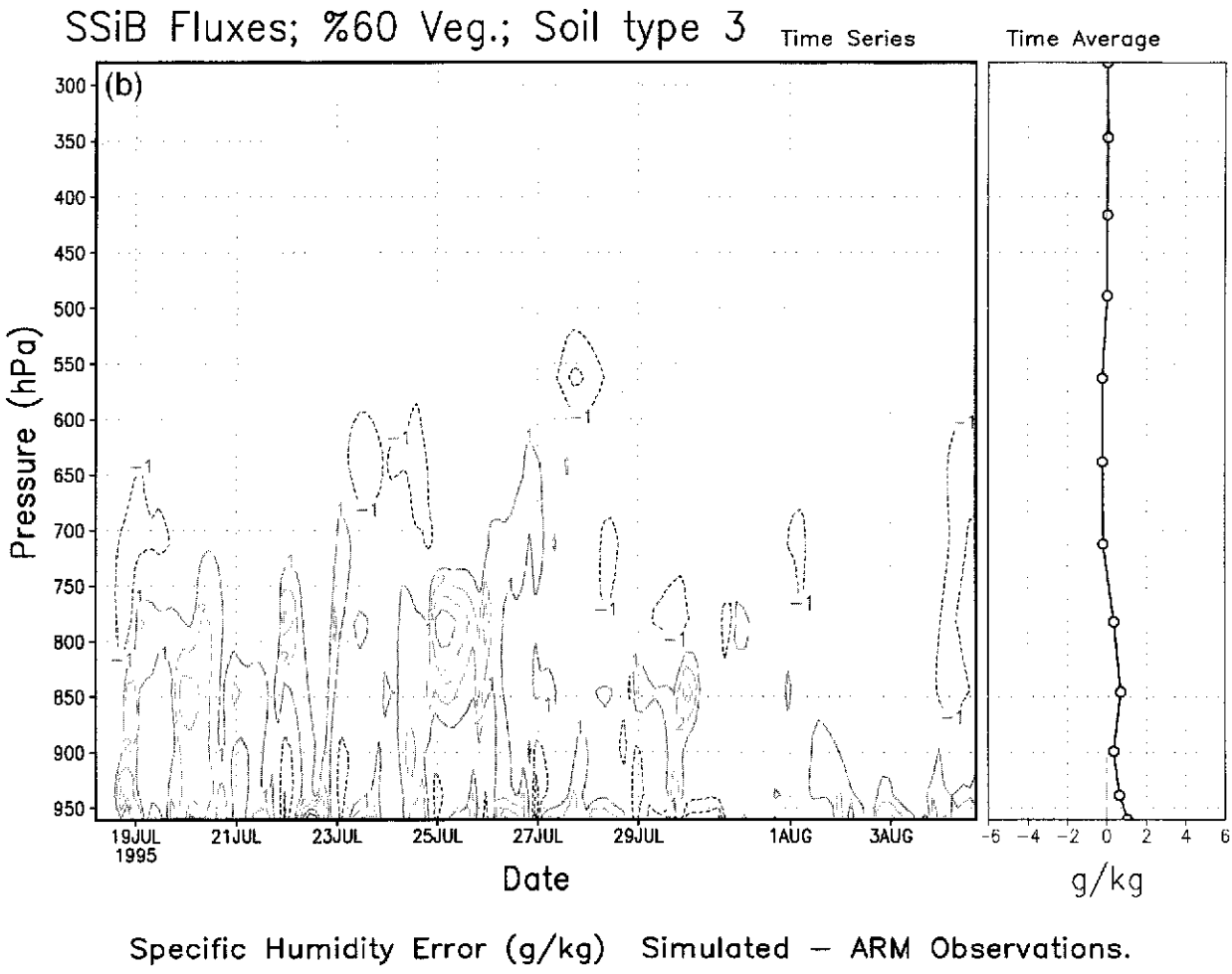

FIG. 7. (*Continued*)

that in turn could affect evapotranspiration and its influence on precipitation.

a. Control simulation

We use (7) and (8) for adjusting the outflow of moisture from the test region in response to the differences in the simulated and observed humidities (and temperatures). Since changes in land surface fluxes would produce corresponding anomalies in the atmospheric water vapor (and temperature), such adjustments are central for simulating the influence of changes in local surface fluxes on rainfall. We simulated each of the four ARM–CART datasets giving the earth–atmosphere system response to 30 combinations of soil types and vegetation cover given in Table 1 and Fig. 3b. The initial soil moisture profiles were determined from an over-6-month (1 January through the starting date of the simulation) soil moisture spinup forced with 1987 ISLSCP Initiative-I data using the prescribed soil types and vegetation fraction. Figures 7a–c show the temperature, relative humidity, and precipitation errors (simulated minus observed) at 3-h intervals for case 1, soil type 3, and 60% vegetation cover (a combination nearest to the observed local conditions). All other diagnostics akin to those discussed in Sud and Walker (1999) were examined and found reasonable; but here we discuss those that could be verified against observations. Using the same SCM, but with surface fluxes prescribed from ARM–CART observations and with no adjustment to the tendencies, yielded reasonably realistic temperature, humidity, and rainfall fields (Figs. 2a–c). Recall that the current simulation is fully interactive and has the surface atmospheric column affecting the divergent outflow and with SSiB coupled to a 100-layer subsoil hydrological model (Koster et al. 2000). Naturally, the simulation generates its own prognostic surface fluxes. Thus the atmospheric simulation contains an adjustment for model errors as well as surface flux anomalies as discussed in section 2. With these adjustments, the simulation yields even more realistic time-mean atmospheric soundings, that is, time series of the vertical profiles of

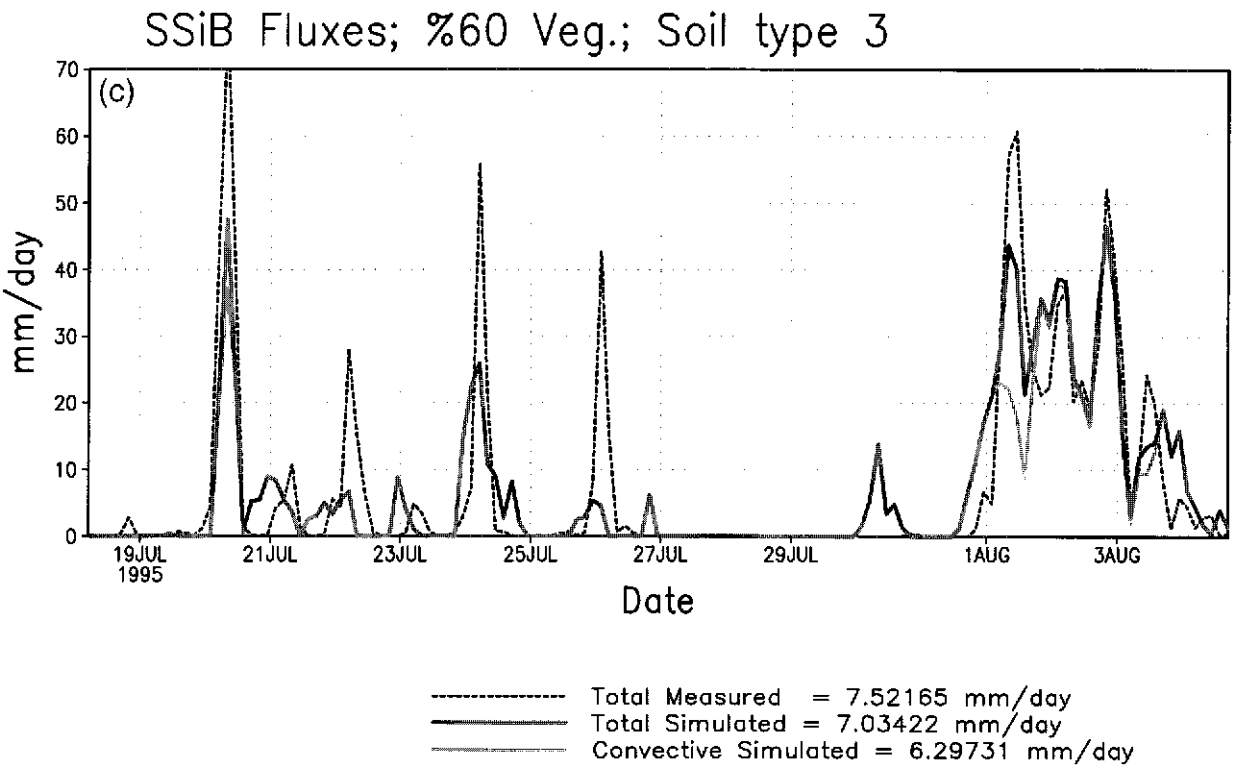

FIG. 7. (*Continued*)

temperature (Fig. 7a) and humidity (Fig. 7b), but without much impact on rainfall (Fig. 7c). In the 3-week averages, (shown on the far right of each panel of Fig. 7), the simulated time-mean biases are at an acceptable level. The instantaneous biases fluctuate around the mean. We note that there are two episodes of about 4°C cooling with a preponderance of 1°–2°C warm (cool) patches at around 100 (400) hPa level, respectively. As noted before, the near-surface air is generally warmer than observed. In the humidity field too, minimal systematic biases appear. However, one could infer that near the surface the model atmosphere is a bit too warm and humid, which compensates for somewhat cooler environments atop. Nevertheless, recognizing that the systematic biases in temperature and humidity are small and stable, we submit that the SCM simulations capture reality of the atmosphere reasonably. Since the simulated precipitation is somewhat less than the observed (Fig. 7c), it implies either the simulated evaporation is too low or the horizontal moisture flux divergence is too high. In fact, the evapotranspiration was quite realistic with the 60% vegetation cover, and therefore the horizontal moisture divergence is likely in error, and this could be due to a model bias and/or the input data. Because these errors do not relate to any systematic errors in the accompanying fields, we argue that the model is performing well within the limits of observational errors. Additional evaluations (not shown) indicate that the choice of a relative humidity trigger for the onset of moist convection is the only parameter that can affect the rainfall amount, but this had no effect on the overall conclusions of this study. Since this trigger can be easily tuned (not done) to get better agreement with observations, we reiterate that despite the aforestated model biases, our SCM evaluations should lead to a robust conclusion.

The evapotranspiration and sensible heat flux time series for three vegetation covers for case 1 with soil type 3 is shown in Figs. 8a and 8b. The plots show observations and three vegetation cover (1%, 60%, and 99% vegetation) cases represented by solid and dashed lines, respectively. There is a considerable overlap between the curves, making them indistinguishable from each other as well as from observations. Clearly, some differences between the observed and simulated surface fluxes cannot be explained by vegetation variations, but recognizing that the SCM has its own clouds that do advect horizontally, moist processes, and radiation parameterizations, the simulated fluxes can be considered reasonable particularly because they depict good diurnal amplitudes and phases. The main purpose of showing them here is to convince the reader that the current SCM can simulate realistic surface fluxes and can respond to cloudy episodes that suppress surface fluxes by shielding of solar radiation. During a particular 5-day dry episode, 26–30 July 1995, the simulated sensible flux

(evapotranspiration) is less (more) than the observed. This suggests that the parameterized vegetation simulated more evapotranspiration even though the simulated rainfall was less. This is of some concern because it may point to a deficiency of the land model or to biases in the initial soil moisture profile (initialized with 1987 data), but the overall temporal structure of evapotranspiration is otherwise quite reasonable. Our model produces some discrepancies in the simulated precipitation time series (Fig. 8c), but the results can be considered satisfactory despite the fact that the 3-week mean precipitation is underestimated.

b. Other simulations

In addition to the control cases, four more sets of simulations were performed with arbitrarily reduced initial soil moisture. The reductions were 25%, 50%, 75%, and 100% of the soil moisture deficit (defined in section 3) of the control case(s). However, the soil moisture was not allowed to go below a small arbitrary value. In this way, a total of 150 simulations for each case were used to establish the robustness of our findings to the initial soil moisture using arbitrary soil moisture anomalies as discussed above.

1) EVAPOTRANSPIRATION

Figure 9 shows that the simulated evapotranspiration for case 1 is a strong function of vegetation cover and soil type for the entire 3-week period. The evaporation is highest for soil type 5 and lowest for soil type 1. The relative patterns are robust regardless of the initial soil moisture—whether they are taken from the spinup initialization for each vegetation cover or from initial soil moisture for the 60% vegetation cover case. The hydrologic characteristics of different soil types are distinguished mainly by soil water suction potential ψ, and soil hydraulic conductivity κ, as a function of soil moisture fraction:

$$\psi = \psi_s f_w^{-B}, \quad \text{and} \tag{10a}$$

$$\kappa = \kappa_s f_w^{2B+3}, \tag{10b}$$

where ψ_s and κ_s are the corresponding saturated soil values, f_W is the soil moisture fraction, and B is the Clapp and Hornberger (1978) parameter. An increase in evapotranspiration for a larger vegetation cover would be expected naturally, but its dependence on soil type is determined by ψ_s and B functions (Table 1). The only major exception is soil type 5, for which the evapotranspiration reduces for 80% and 99% vegetation cover. This presumably is the result of nonlinear stomatal control of vegetation to soil moisture, ambient temperature, and the photosynthetically active radiation (PAR). The accompanying sensible fluxes (not shown) were consistent with the surface energy balance and do not have large variations (Table 2). We naturally expect sensible fluxes to decrease with increasing vegetation cover, but the problem is complicated by the amount of solar energy absorption at the surface through the surface albedo α_{surf}, which itself is a function of vegetation cover:

$$\alpha_{\text{surf}} = V_f \alpha_{\text{forest}} + (1 - V_f)\alpha_{\text{desert}}. \tag{11}$$

Moreover, the transpiration characteristics are modulated by the limiting influence of wilting for low levels of root-zone soil moistures. These lead to a slight increase in sensible fluxes with increased vegetation, particularly for soil type 3.

2) PRECIPITATION

For case 1, the dependence of precipitation on evapotranspiration, caused by changes in vegetation cover and soil type, clearly affirm the qualitative inferences of Sud et al. (1993, 1995) and Schickendanz and Ackermann (1977). The simulated precipitation variations are shown on the right-hand panels of Fig. 9. The precipitation increases with increased vegetation cover as well as evapotranspiration presumably due to increased moisture supply through evaporation. The evapotranspiration decrease for soil type 5, 80% vegetation cover yields a corresponding decrease in precipitation. The spread among the different soil types becomes less as vegetation cover increases. As expected, for high vegetation cover (e.g., 99%), both the evaporation and precipitation for all soil types tend to be closer. This suggests that the influence of the soil type on evapotranspiration is suppressed as vegetation begins to control the surface energy budget and evaporation, both of which influence rainfall. We reiterate here that we match evapotranspiration quite well with observations, but the simulated precipitation continues to be somewhat less than the observed. This error does not seem to be related to moisture storage in the atmosphere because the model has been found to simulate realistic temperatures and specific humidity profiles (see section 4a). Hence, the discrepancy must emanate from the prescribed (ARM CART) data or the model bias correction for the horizontal advection [(5); section 2]. Nevertheless, for a given vegetation cover, clearly the soils that produce more evapotranspiration also produce more precipitation.

3) VEGETATION–EVAPORATION–PRECIPITATION

Now we employ all the ARM–CART cases to develop the evapotranspiration–precipitation relationship as a function of vegetation cover. Figure 10 shows the results for each ARM–CART case averaged over all soil types. Evaporation increased with vegetation cover for cases 1, 3, and 8. Surprisingly for case 4, it decreased with vegetation cover. We investigated the cause of such a behavior. First, case 4 is for a September IOP; in this period, the root zone was already dry and vegetation was unable to generate much transpiration. Besides, the

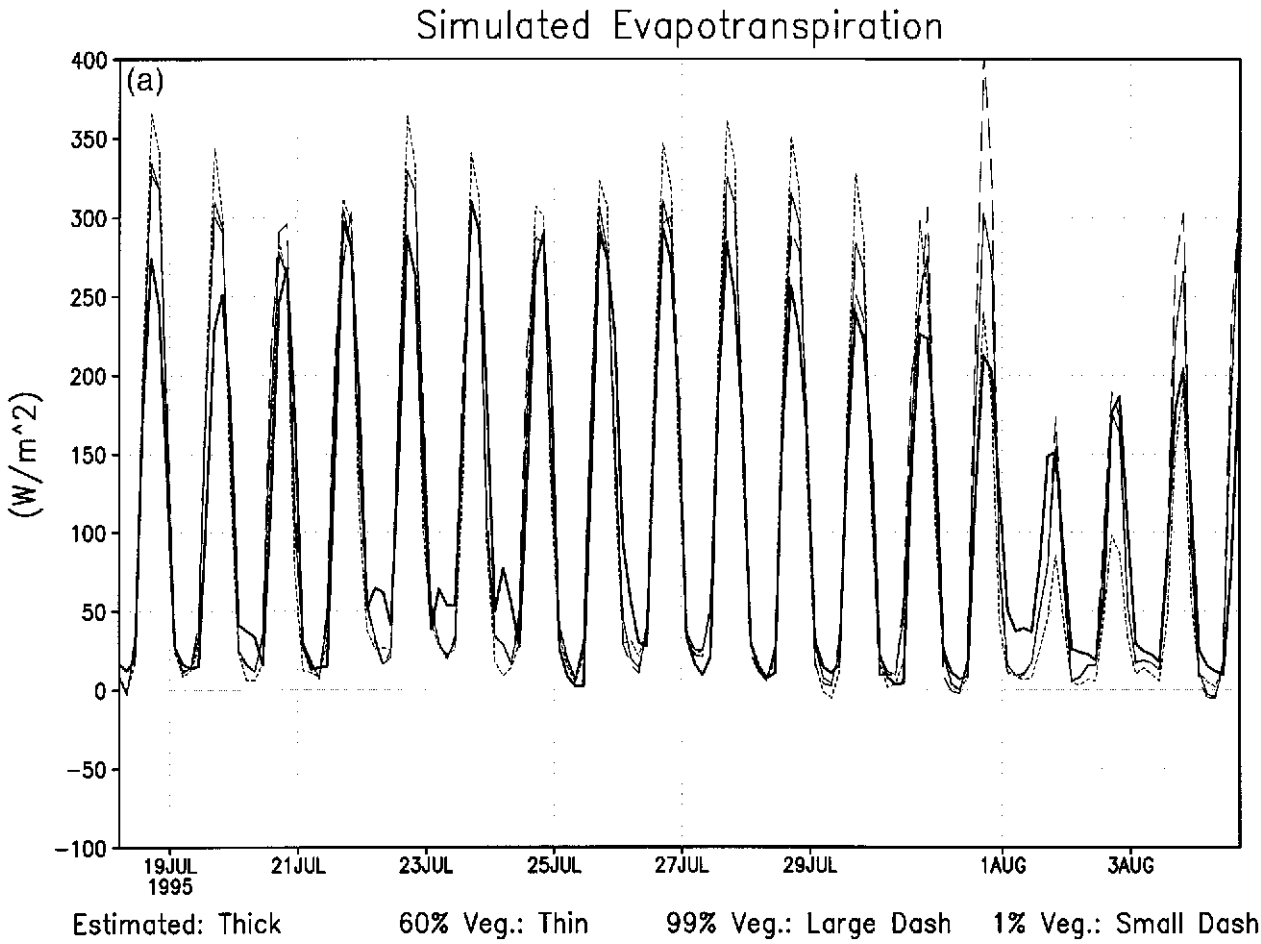

FIG. 8. Case-1 simulated vis-à-vis observed fluxes of (a) evapotranspiration and (b) sensible heat for soil type 3. The four lines are for 1%, 60%, and 99% vegetation covers vs observations, which correspond to roughly 60% vegetation cover. The corresponding precipitation fields are in (c).

near-autumn vegetation lacked the ability to transpire as much. In fact, more evaporation occurred from the top layer of soil as soil evaporation. With increased vegetation cover, the soil evaporation naturally got reduced while the transpiration could not increase much. The combined effect was to generate reduced total evapotranspiration for increased vegetation cover. However, for the 60% initial soil moisture (bottom left, Fig. 10) we see this behavior changes and there is an increase in evaporation, however slight, with vegetation for all cases including case 4; nevertheless, there is much less evaporation.

Averaged across all soils, case 1 (a wet case) shows much more increase in precipitation with an increase in vegetation cover, whereas cases 3 and 4 with near-normal rainfall show an indifferent influence, while case 8, with a strong drought circulation, continues to maintain the drought for both initial soil moisture values (normal and 60%). These results reveal that the large-scale circulation has a strong influence on the SCM-simulated precipitation. In addition, the lack of vertical velocity feedback to changes in diabatic heating of the column atmosphere may have a tendency to increase the column's humidity interaction and/or transport into horizontal divergence. Table 2 shows that for case 4 the evapotranspiration drops while the sensible flux increases warming the near-surface air; this is likely to further stifle evapotranspiration.

4) EVAPORATION–PRECIPITATION RELATIONSHIP

Figure 11 shows the IOP-averaged evaporation–precipitation plot for all the 150 simulations regardless of the interplay between vegetation, soil moisture, soil type, and surface energy balance as four curves for each of the four ARM–CART cases. We see that the atmosphere responds to evaporation change in a robust fashion regardless of the complexity of the biospheric processes and land hydrology. This response is delightfully simple and linear. It shows that for the Great Plains

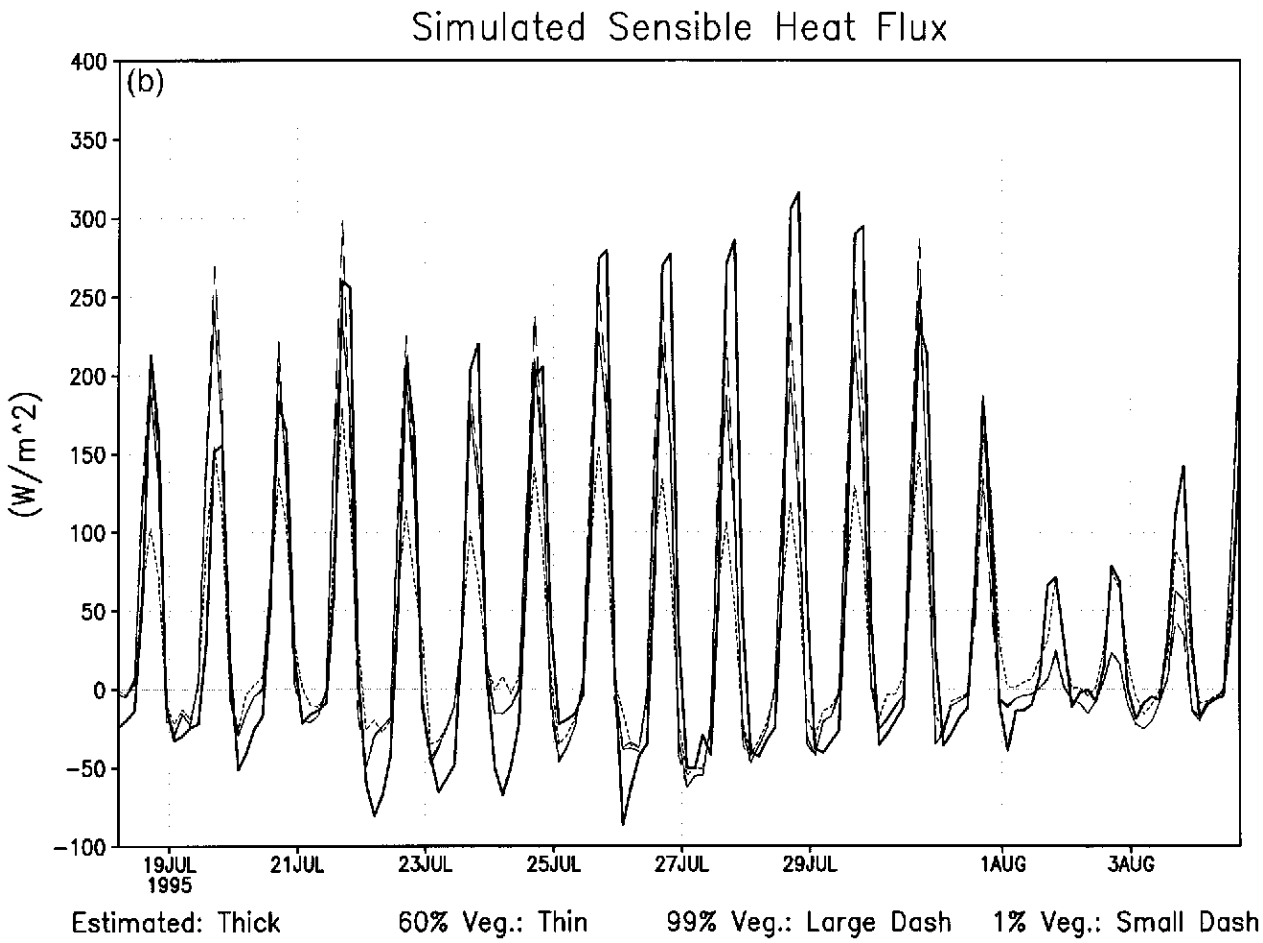

FIG. 8. (*Continued*)

region, roughly 50%, 25%, 7%, and 0.5% of the evapotranspiration would be returned back in the form of increased precipitation for cases 1, 3, 4, and 8, respectively. A linear regression analysis gave a slope of 0.499, 0.242, 0.073, and 0.005, respectively (see Table 3). We attempted to verify the precipitation intercepts (*b* value) by running one simulation for each of the four cases with dry soil at the initial time. The simulation produced some evaporation through rainfall interception and soil surface wetting produced during the course of the integration. The simulated evaporation–precipitation (large black dots) reaffirmed with the linear fit relationship quite well. Consequently, we contend that even though the evaporation over the ARM–CART site is complicated by soil type, soil moisture, and vegetation characteristics (i.e., PAR, temperature, ambient humidity, and winds affecting transpiration), the evaporation–precipitation relationship is relatively straightforward and depends upon the background circulation used to force the SCM laterally. Broadly, for wet conditions, the evapotranspiration produces a strong feedback effect on rainfall, whereas for drought circulation, the influence can be inconsequential.

5) MOISTURE DISTRIBUTION IN THE VERTICAL

(i) Vegetation dependence

Among the four cases studied, case 1 produces the strongest influence of surface fluxes on precipitation; therefore it is analyzed further to better understand the response of the atmosphere. The vertical structure of moisture divergence has some interesting features as shown in Fig. 12a. With increasing vegetation cover, the moisture divergence becomes smaller near the surface, that is, between 960 (surface pressure) and 850 hPa. However, it increases for the middle atmosphere (i.e., between 500 and 850 hPa) despite larger evapotranspiration adding moisture to the lower troposphere. Such an outcome might be due to enhanced upward transport of moisture by physical processes and/or its removal by low-level condensation, which was found to be small. An increase in moisture divergence in the middle atmosphere represents the influence of moist convection and dry turbulent exchanges. The outcome could be naturally complicated by surface albedo decreases for higher vegetation cover. Indeed, larger surface energy fluxes would amount to larger moist static

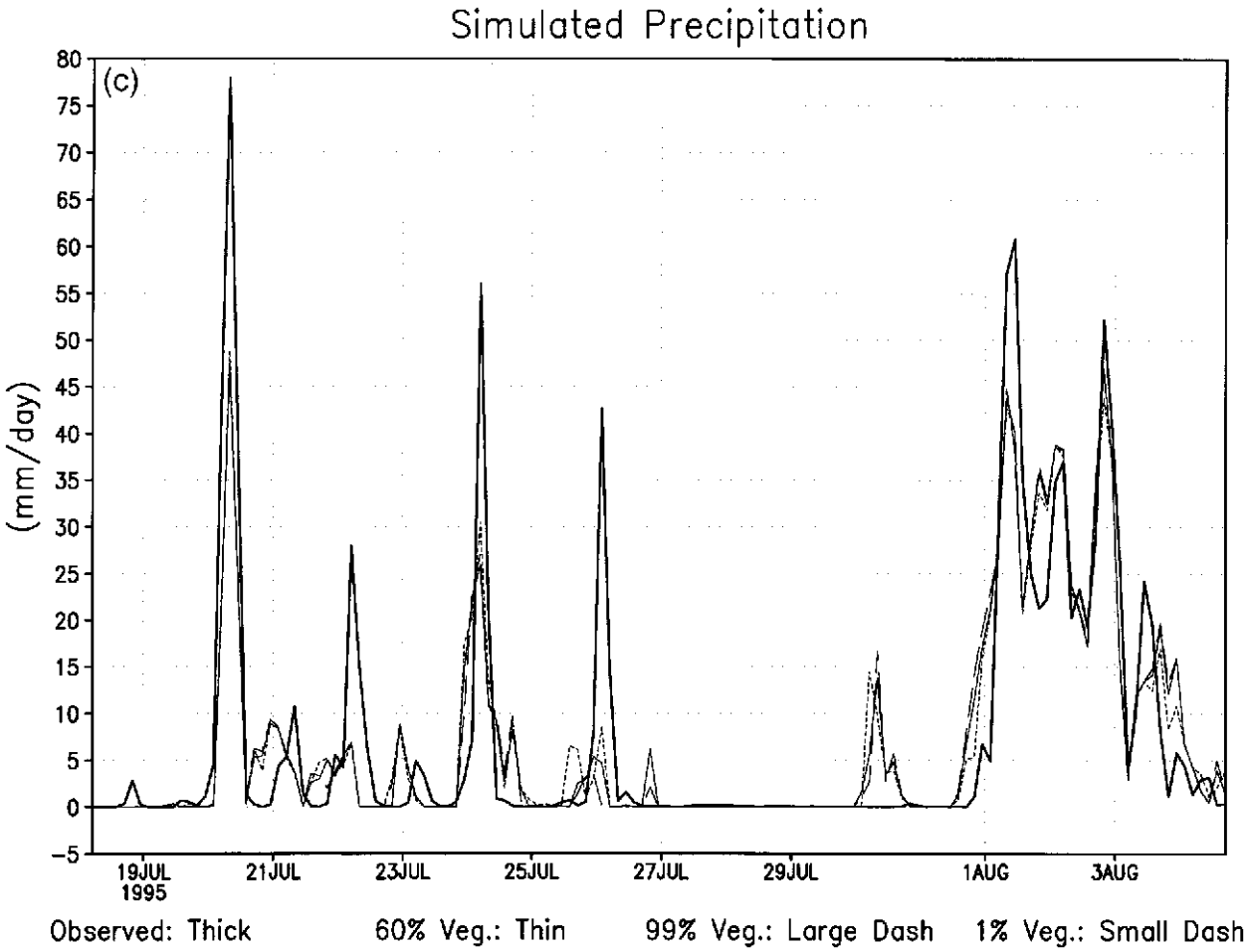

FIG. 8. (*Continued*)

TABLE 2. Time-averaged fluxes and precipitation at the surface.

Simulation period and ARM–CART case No.	Vegetation fraction	Surface fluxes (W m^{-2})			Precipitation (mm day^{-1})
		Net radiation	Evapotranspiration	Sensible heat	
18 Jul–4 Aug 1995	Data*	149.1	110.0	44.6	7.52
Case 1	1%	143.5	109.0	28.9	6.94
	60%	158.1	115.0	38.8	7.03
	99%	164.1	118.9	41.6	7.06
19 Jun–18 Jul 1997	Data*	163.1	123.1	33.4	4.34
Case 3	1%	158.2	124.7	27.0	3.55
	60%	171.6	121.6	44.5	3.34
	99%	179.6	124.2	51.2	3.28
15 Sep–6 Oct 1999	Data*	102.6	68.5	34.8	3.67
Case 4	1%	85.2	75.2	7.22	3.02
	60%	84.4	53.7	28.4	2.88
	99%	86.7	50.8	35.5	2.87
12 Jul–22 Jul 1999	Data*	182.7	126.2	34.3	0.856
Case 8	1%	156.0	126.3	25.2	0.0266
	60%	172.0	122.4	45.7	0.0181
	99%	177.8	121.5	52.9	0.0163

* ARM–CART data provided as best estimate of observation.

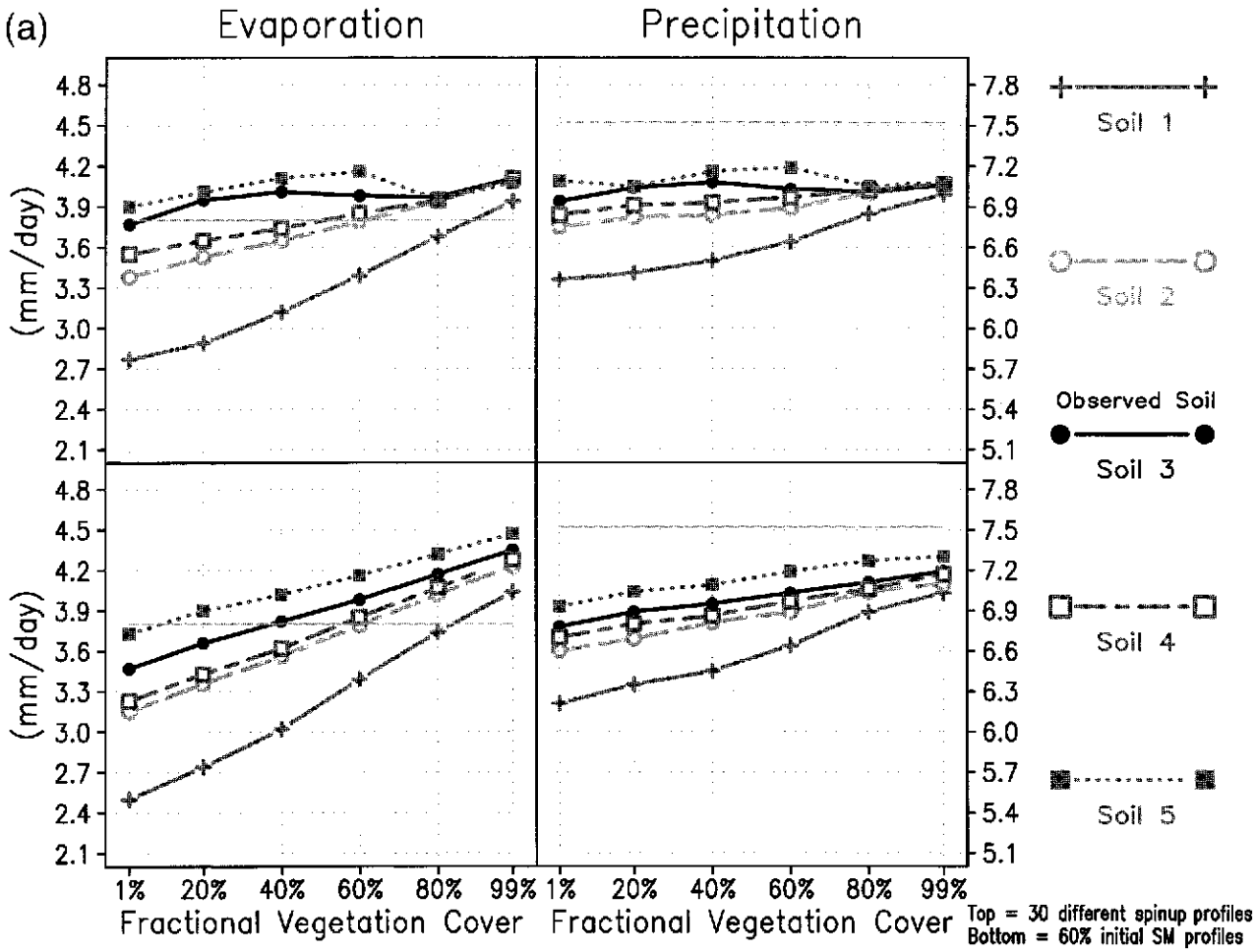

FIG. 9. Simulated (left) evaporation and (right) precipitation as a function of vegetation fraction for the entire period for each of the five soil types for case 1 using (top) 30 different soil moisture spinup profiles and (bottom) 60% initial soil moisture profiles.

energy and invigorated moist convection. Moreover, during the spinup, the land with lower vegetation cover naturally transpires less and retains more precipitation as soil moisture; in this way it tries to mitigate transpiration reduction by direct soil evaporation. Since an atmospheric layer, moistened with evaporation, is expected to produce larger moisture divergence, the simulated reduction in moisture divergence suggests the dominant role of upward moisture transport by physical processes. Not only does the moist convection transport the cloud sublayer moisture upward, but it also brings dry air into the surface layers through convective-scale downdrafts. To the extent that the moisture loss of the lower layer is reflected as moisture gain in the middle layer or even the top layer (which is miniscule), the peculiar behavior in Fig. 12a is an outcome of the vertical transport. Indeed, when we assumed the depth of the lowest layer to 700 mb, most of the moisture divergence changes were reflected in that layer (not shown). Because of this, we argue that surface fluxes can affect the vertical transport of moisture through boundary layer and moist convective processes. Our SCM simulations reveal that despite the evaporation increase, the lower layers can be drier.

(ii) Evapotranspiration dependence

Case-1 simulations were also used to analyze the relationship between near-surface moisture divergence and evapotranspiration. The IOP-averaged plot in Fig. 12b shows a discernible scatter because the surface energy absorption is a function of vegetation cover, which also influences the surface evaporation. As expected, the moisture divergence reduces (becomes less negative) as evapotranspiration increases. This is obviously different from its relationship with vegetation cover where it reduced with vegetation cover that leads to evaporation increase. The upper-level moisture divergences, that is, 850–200 hPa (not shown), have compensating (opposite sign) effects on the moisture divergence simulated in the near-surface layers (shown in Fig. 12a). The sum of the entire column moisture divergences

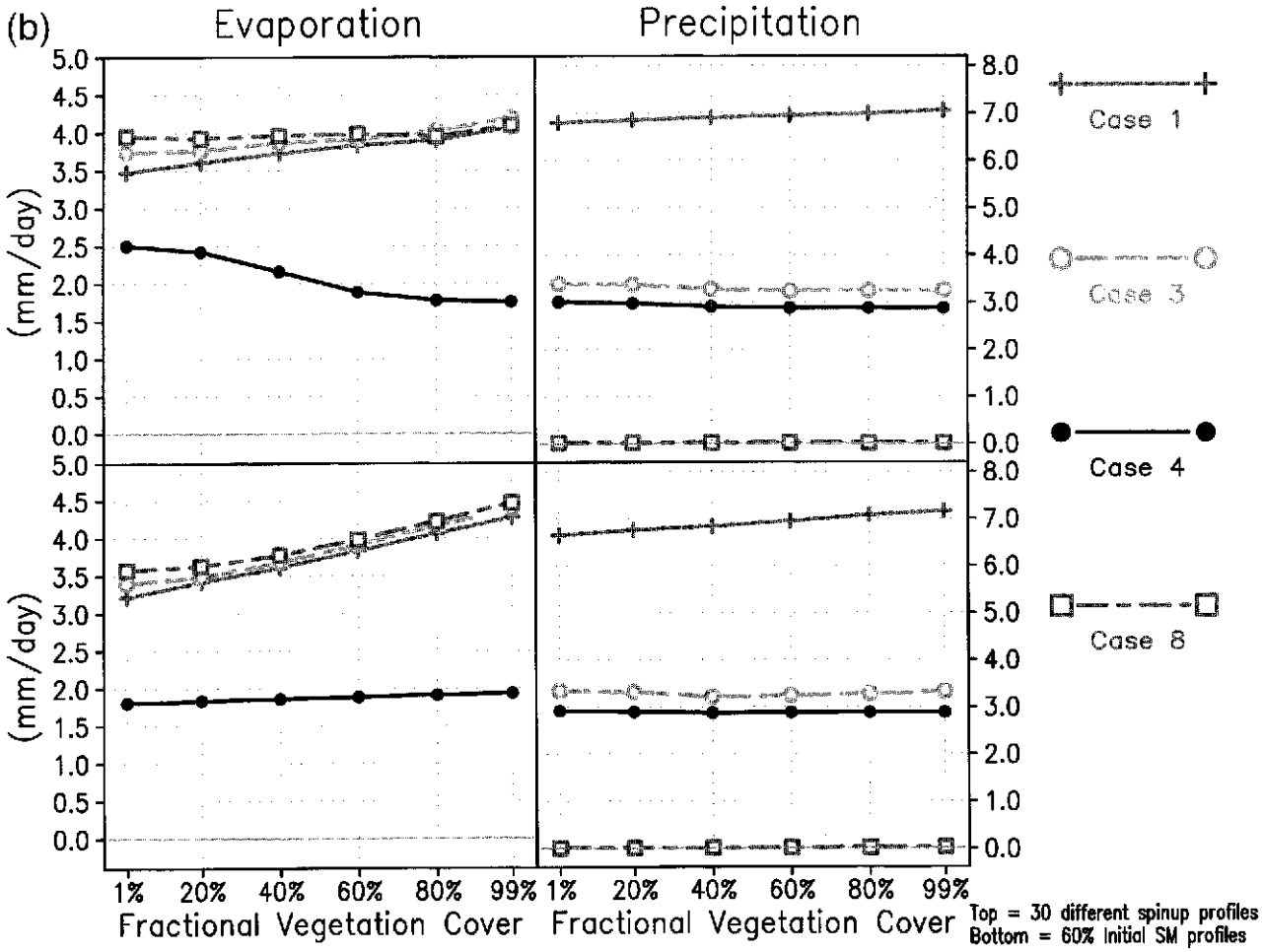

FIG. 10. Simulated (left) evaporation and (right) precipitation as a function of vegetation fraction for the entire period averaged for all soil types using (top) 30 different soil moisture spinup profiles and (bottom) 60% initial soil moisture profiles.

yields a smooth graph showing a linear relationship between moisture divergence and evapotranspiration. This is also consistent with a linear relationship between simulated precipitation and evapotranspiration (Fig. 11).

5. Discussion and conclusions

The aim of the current investigation was to understand how vegetation cover, soil type, and soil moisture could influence rainfall in the midwestern United States during summer season. Four ARM–CART SCM datasets (one for June, two for July, and one for September IOPs) were deployed to run an SCM version of the GEOS-2 GCM. If the precipitation were weakly affected by surface fluxes, the rainfall in the region would be largely independent of evapotranspiration. One can intuitively infer that the Sahara Desert and/or coastal regions with orographic lifting and inland large-scale flow would be such regions. Nevertheless, the evapotranspiration–precipitation feedback could vary depending upon the region and/or the large-scale pattern of the atmospheric circulation; such an understanding would enable one to influence the local precipitation by clever management of the biosphere.

The current SCM simulations with the ARM–CART data confirm a positive feedback between evapotranspiration and precipitation. This relationship is strong for wet conditions and is truly weak for a drought circulation. We simulate larger evapotranspiration in the growing season in response to higher initial vegetation cover. To use these results under field conditions, the extra water needed for increasing the evapotranspiration would have to be supplied through irrigation that relies on external water sources or ground water storage. However, because of the evapotranspiration–rainfall relationship and efficient retention of rainwater by the vegetation in the biosphere, the external water supply could be only one-half to three-quarters of that needed for enhanced evapotranspiration. Obviously, these results cannot be generalized to other regions. Even for the Midwest summer, the results are strongly circulation dependent and therefore warrant some caution. In pre-

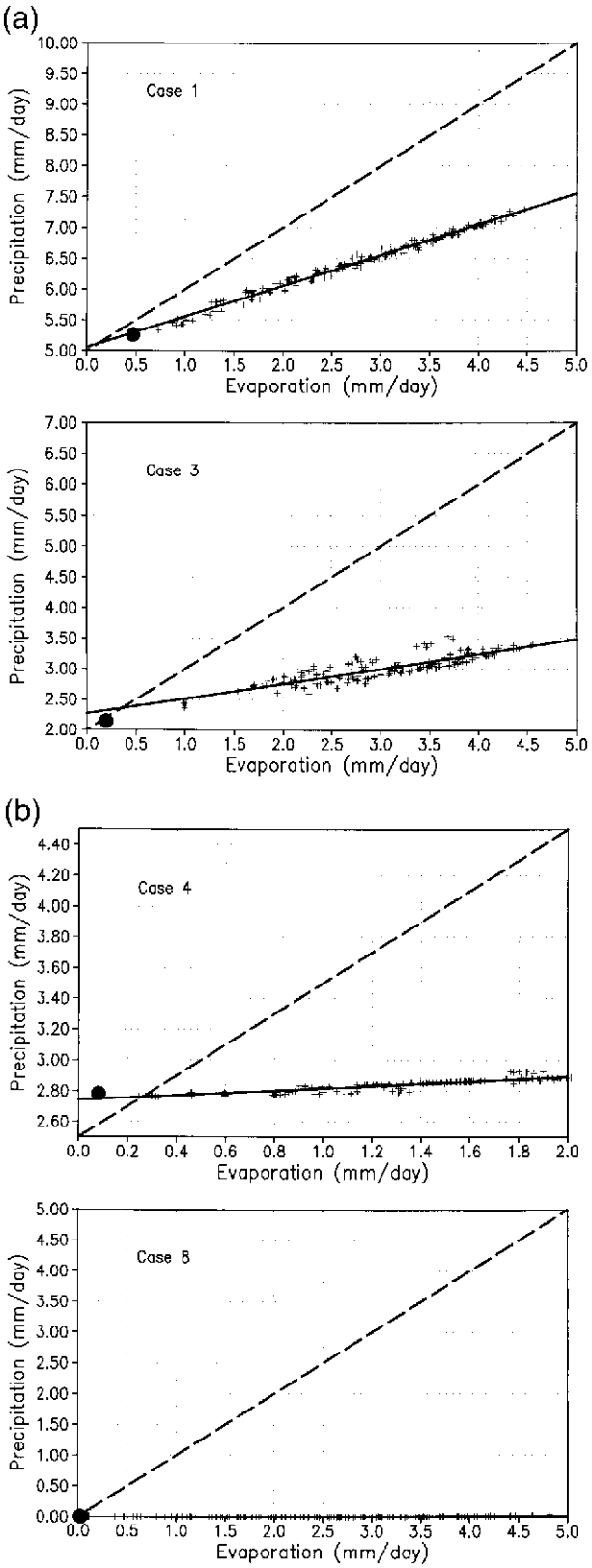

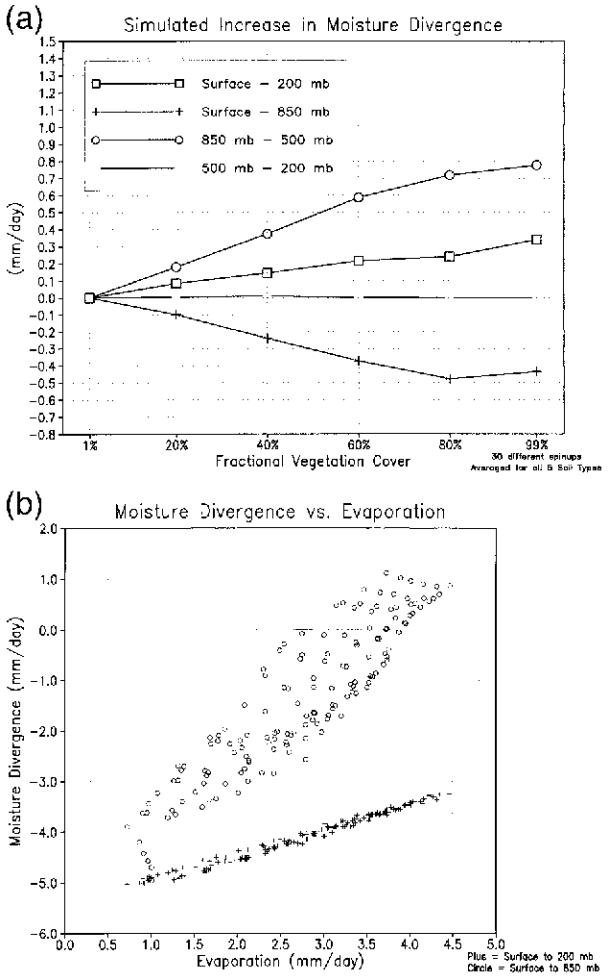

FIG. 12. (a) IOP-averaged simulated moisture divergence increase above the 1% vegetation cover as a function of vegetation cover for case 1 between (i) the surface and 850 hPa, (ii) 850 and 500 hPa, (iii) 500 and 200 hPa, and for (iv) entire column values. (b) Scatterplots of (i) surface–850-hPa moisture divergence and (ii) surface–200-hPa level moisture divergence as a function of surface evaporation regardless of the vegetation fraction or initial soil moisture for case 1.

scribing large-scale lateral forcing for the SCM, we implicitly assume that the regional hydroclimatological changes are not so large as to affect the large scale. This might not hold true for some cases. Nevertheless, we have made an appropriate adjustment for the large-scale forcing of the SCM by introducing a methodology for the grid-scale columnar temperature and humidity

←

FIG. 11. Evaporation–precipitation relationship for an ensemble of five sets. Each set has five soil types, six vegetation covers, and uses an initial soil moisture profile from 60% vegetation cover initialization produced with multimonth spinups. The solid line is a least squares fit to the SCM simulations. The dashed line represents all of the increase in evapotranspiration turning into precipitation. The panels are for cases 1, 3, 4, and 8 as indicated on the panel.

TABLE 3. Least squares fit where $P = aE + b$.

Case No.	a	b	Correlation	Rms error
1	0.499	5.059	0.992	0.060
3	0.242	2.270	0.875	0.114
4	0.073	2.743	0.938	0.018
8	0.005	−0.005	0.823	0.004

changes to affect their advective tendencies in the horizontal as well as the vertical directions. Consequently, we contend that our investigation is a realistic 4-case study in which scale separation between the large and mesoscales has been assumed.

Indeed, the moisture advected out of the SCM will not be a loss for the region as a whole because the water vapor still has a long way to travel before it leaves the continent. It will naturally augment the water vapor content of the air mass flowing out of the region, and it is likely to increase the precipitation in the nearby regions (Schickedanz and Ackermann 1977). Thus, even if the irrigation were to rely on transporting water available a few hundred kilometers around the region, the excess rainfall outside the region would be likely to recover some of the water transported for transpiration by the biosphere.

A natural question is would the vegetation-induced subgrid-scale variability in surface fluxes and moist processes affect the local mesoscale circulation? The answer is indeed it would (Pielke and Avissar 1990); however, the goal of a good parameterization is to handle such effects realistically, particularly in the domain-averaged sense. Whether our SCM invoking GEOS-2 physics and McRAS is adequate enough to address such influences remains unanswered, but the fact that the SCM responds realistically to several ARM–CART and other evaluations provides some credibility to the current studies (Sud and Walker 1999; Ghan et al. 2000). Besides, SSiB and its evapotranspiration submodel have been evaluated thoroughly with several field observations, while the new 100-layer land hydrological model is invoked to improve the hydrologic accuracy of soil water conduction. Therefore, we are convinced that our evapotranspiration and soil hydrological model is as good as that in any state-of-the-art SCM. We believe studies such as this could help to alleviate some of the ambiguity generated by a variety of answers given by GCMs to a typical deforestation such as summarized in Hahmann and Dickinson (1997) and other studies of climatic effects of vegetation and/or soil moisture anomaly scenario.

In addition to the above limitations associated with the evaluation procedure and the modeling assumptions, several inherent parameterization problems continue to hinder an accurate simulation of land–atmosphere interaction. Among the unsolved problems are the influences of subgrid-scale variability of soil type, soil moisture, vegetation cover, and orography. The drainage characteristics and surface runoff pathways with their associated effects on the water table and soil moisture availability are also ignored. A highly nonlinear response of surface fluxes to such variations makes the problem of parameterizing land processes truly hard to address. In addition, the intrinsic variability of biospheric processes, particularly on seasonal and longer timescales, diminishes the positive influences of recent advances on climate simulation although interactive biosphere climate simulations have begun to show promise (Zeng et al. 1999). Under the circumstances, controlled evaluations such as ours may provide an important insight. We plan to continue to test our approach using additional datasets for the Midwest and other important regions of the world.

Acknowledgments. The funding support of our research by Dr. Kenneth Bergman of NASA headquarters is immensely appreciated. Participation of two coauthors, D. M. Mocko and G. K. Walker, was supported by these funds. Dr. W. K.-M. Lau, head of the Climate and Radiation Branch of the Laboratory for Atmospheres, encouraged this research.

REFERENCES

Anthes, R. A., 1984: Enhancement of convective precipitation by mesoscale variations in vegetative covering in semi-arid regions. *J. Climate Appl. Meteor.,* **23,** 541–554.

Arakawa, A., and W. H. Schubert, 1974: Interaction of a cumulus ensemble with the large-scale environment. Part I. *J. Atmos. Sci.,* **31,** 674–701.

Avissar, R., 1992: Conceptual aspects of a statistical-dynamic approach to represent landscape subgrid-scale heterogeneities in atmospheric models. *J. Geophys. Res.,* **97** (D3), 2729–2742.

Cheng, M.-D., 1989: Effects of downdrafts and mesoscale convective organization on the heat and moisture budgets of tropical cloud clusters. Part I: A diagnostic cumulus ensemble model. *J. Atmos. Sci.,* **46,** 1517–1538.

Clapp, R. B., and G. M. Hornberger, 1978: Empirical equations for some soil hydraulic properties. *Water Resour. Res.,* **14,** 601–604.

Dickinson, R. E., 1980: Effect of tropical deforestation on climate. Blowing in the wind: Deforestation and long range implication, studies in the third world societies. Department Anthropology, College of William and Mary Publication No. 14, 411–441.

——, and A. Henderson-Sellers, 1988: Modeling tropical deforestation: A study of GCM land surface parameterizations. *Quart. J. Roy. Meteor. Soc.,* **114,** 439–462.

Dirmeyer, P. A., and J. Shukla, 1994: The effect on climate of doubling deserts. Center for Ocean–Land–Atmosphere Studies Report No. 3, 32 pp. [Available from Center for Ocean–Land–Atmosphere Studies, 4041 Powder Mill Road, Suite 302, Calverton, MD 20705-3106.]

——, A. J. Dolman, and N. Sato, 1999: The pilot phase of the Global Soil Wetness Project. *Bull. Amer. Meteor. Soc.,* **80,** 851–878.

Eltahir, E. A. B., and R. L. Bras, 1993: On the response of tropical atmosphere to large-scale deforestation. *Quart. J. Roy. Meteor. Soc.,* **119,** 779–793.

Ghan, S. J., and Coauthors, 2000: A comparison of single column model simulations of summertime midlatitude continental convection. *J. Geophys. Res.,* **105** (D2), 2091–2124.

Hahmann, A. N., and R. E. Dickinson, 1997: RCCM2–BATS model over tropical South America: Applications to tropical deforestation. *J. Climate,* **10,** 1944–1964.

Henderson-Sellers, A., R. E. Dickinson, T. B. Durbidge, P. J. Kennedy, K. McGuffie, and A. J. Pitman, 1993: Tropical deforestation—Modeling local-scale to regional-scale climate change. *J. Geophys. Res.,* **98** (D4), 7289–7315.

Hoffert, M. I., and Y. C. Sud, 1976: Similarity theory of the buoyantly interactive planetary boundary layer with entrainment. *J. Atmos. Sci.,* **33,** 2136–2151.

Koster, R. D., and P. S. Eagleson, 1990: A one-dimensional interactive soil–atmosphere model for testing formulations of surface hydrology. *J. Climate,* **3,** 593–606.

——, and M. J. Suarez, 1999: A simple framework for examining the interannual variability of land surface moisture fluxes. *J. Climate,* **12,** 1911–1917.

——, ——, A. Ducharne, M. Stieglitz, and P. Kumar, 2000: A catchment-based approach to modeling land surface processes in a general circulation model. Part I: Model structure. *J. Geophys. Res.,* **105,** 24 809–24 822.

Mocko, D. M., and Y. C. Sud, 1998: Comparison of land surface model (SSiB) to three parameterizations of evapotranspiration—A study based on the ISLSCP Initiative I data. *Earth Interactions,* **2.** [Available online at http://EarthInteractions.org.]

——, and ——, 2001: Refinements to SSiB with an emphasis on snow-physics: Evaluation and validation using GSWP and Valdai data. *Earth Interactions,* in press.

Moorthi, S., and M. J. Suarez, 1992: Relaxed Arakawa–Schubert: A parameterization of moist convection for general circulation models. *Mon. Wea. Rev.,* **120,** 978–1002.

Nicholson, S. E., 1985: Sub-Saharan rainfall 1981–1984. *J. Climate Appl. Meteor.,* **24,** 1388–1391.

Otterman, J., A. Manes, S. Rubin, P. Albert, and D. O'C. Starr, 1990: An increase of early rains in southern Israel following land-use change. *Bound.-Layer Meteor.,* **53,** 331–351.

Pielke, R. A., and R. Avissar, 1990: Influence of landscape structure on local and regional climate. *Landscape Ecol.,* **4,** 133–155.

Randall, D. A., and D. G. Cripe, 1999: Alternative methods for specification of observed forcing in single-column models and cloud system models. *J. Geophys. Res.,* **104,** 24 527–24 545.

——, K.-M. Xu, R. J. C. Somerville, and S. Iacobellis, 1996: Single column models and cloud ensemble models as links between observations and climate models. *J. Climate,* **9,** 1683–1697.

Schickedanz, P. T., and W. C. Ackermann, 1977: Influence of irrigation on precipitation in semi-arid climates. *Arid Land Irrigation in Developing Countries.* E. B. Worthington, Ed., Pergamon Press, 185–196.

Skole, D., and C. Tucker, 1993: Tropical deforestation and habitat fragmentation in the Amazon: Satellite data from 1978 to 1988. *Science,* **260,** 1905–1910.

Sud, Y. C., and M. J. Fennessy, 1982: A study of the influence of surface-albedo on July circulation in semi-arid regions using the GLAS GCM. *J. Climatol.,* **2,** 105–125.

——, and ——, 1984: A numerical study of the influence of evaporation in semi-Arid regions on the July circulation. *J. Climatol.,* **4,** 383–398.

——, and W. E. Smith, 1985: Influence of local land-surface processes on the Indian monsoon: A numerical study. *J. Climate Appl. Meteor.,* **24,** 1015–1036.

——, and A. Molod, 1988: A GCM simulation study of the influence of Saharan evapotranspiration and surface-albedo anomalies on July circulation and rainfall. *Mon. Wea. Rev.,* **116,** 2388–2400.

——, and G. K. Walker, 1993: A rain-evaporation and downdraft parameterization to complement a cumulus updraft scheme and its evaluation using GATE data. *Mon. Wea. Rev.,* **121,** 3019–3039.

——, and ——, 1999: Microphysics of clouds with the Relaxed Arakawa–Schubert scheme (McRAS). Part I: Design and evaluation with GATE Phase III data. *J. Atmos. Sci.,* **56,** 3196–3220.

——, J. Shukla, and Y. Mintz, 1988: Influence of land surface roughness on atmospheric circulation and rainfall: A sensitivity study with a general circulation model. *J. Appl. Meteor.,* **27,** 1036–1054.

——, W. C. Chao, and G. K. Walker, 1993: Dependence of rainfall on vegetation: Theoretical considerations, simulation experiments, observations, and inferences from simulated atmospheric soundings. *J. Arid-Environ.,* **25,** 5–18.

——, K.-M. Lau, G. K. Walker, and J. H. Kim, 1995: Understanding biosphere–precipitation relationships: Theory, model simulations, and logical inferences. *MAUSAM,* **46,** 1–14.

Sundqvist, H., 1988: Parameterization of condensation and associated clouds in models for weather prediction and general circulation simulation, Part I. *Physically Based Modelling and Simulation of Climate and Climatic Change,* M. E. Schlesinger, Ed., Reidel, 433–461.

——, 1993: Inclusion of ice-phase of hydrometeors in cloud parameterization of large-scale and meso-scale models. *Contrib. Atmos. Phys.,* **66,** 137–147.

——, E. Berge, and J. E. Kristjánsson, 1989: Condensation and cloud parameterization studies with a mesoscale numerical weather prediction model. *Mon. Wea. Rev.,* **117,** 1641–1657.

Walker, G. K., Y. C. Sud, and R. Atlas, 1995: Impact of the ongoing Amazonian deforestation on local precipitation: A GCM simulation study. *Bull. Amer. Meteor. Soc.,* **76,** 346–361.

Xue, Y.-K., P. J. Sellers, J. L. Kinter, and J. Shukla, 1991: A simplified biosphere model for global climate studies. *J. Climate,* **4,** 345–364.

Zeng, N., J. D. Neelin, K.-M. Lau, and C. J. Tucker, 1999: Enhancement of interdecadal climate variability in the Sahel by vegetation interaction. *Science,* **286,** 1537–1540.

Zhang, M. H., and J. L. Lin, 1997: Constrained variational analysis of sounding data based on column-integrated budgets of mass, heat, moisture, and momentum: Approach and application to ARM measurements. *J. Atmos. Sci.,* **54,** 1503–1524.